Construction and Building Materials 521 (2026) 146143

Contents lists available at ScienceDirect

Construction and Building Materials

journal homepage: www.elsevier.com/locate/conbuildmat

Comparative assessment of hemp shiv and basalt fibre reinforcements in lime-based mortars for sustainable building and heritage-compatible applications

Elif Çam, Loucas Kyriakou, José María Fernández, Íñigo Navarro-Blasco, José Ignacio Álvarez *

MATCH Research Group, Department of Chemistry, School of Sciences, University of Navarra, C/. Irunlarrea 1, Pamplona 31008, Spain

ARTICLE INFO

Keywords:
Basalt Fibre
Hemp Shiv
Natural Hydraulic Lime
Air Lime
Ternary Mortars
Mechanical Performance
Thermal Conductivity

ABSTRACT

The need to enhance both the mechanical resistance and the thermal performance of lime mortars has intensified interest in fibre-based reinforcement strategies, particularly for heritage-oriented and energy-efficient construction. This study evaluates the influence of natural and mineral reinforcements, hemp shiv and basalt fibre, on the fresh state, physical, microstructural, mechanical, and thermal behaviour of three lime-based mortar systems: natural hydraulic lime (NHL), air lime, and a mixed air lime–cement binder. Reinforcements were incorporated at two dosages (1 and 4 wt% of binder) to examine their interaction with distinct binder chemistries and pore structures. Hemp shiv decreased workability and increased open porosity across all mortars, while basalt fibre produced only limited changes in fresh properties. Microstructural variations arose mainly from increased air-void content due to weak binder–fibre adhesion and interfacial gaps. Compressive strength trends reflected these microstructural modifications; natural hydraulic lime mortars achieved the highest values up to 12 MPa, and high-dosage basalt fibre improved long-term strength through crack bridging, whereas hemp shiv reduced strength, particularly at higher dosages, by 21% in NHL mortars and about 60% in air lime-based mortars. Thermal behaviour, however, showed clear benefits across all reinforced mortars: thermal conductivity consistently decreased, with the most significant reductions observed in hemp-shiv mixtures, up to 30%, and in basalt-fibre mortars at low dosage by 45% in NHL mortars and 24% in air lime-based mortars. These improvements highlight the capacity of fibre reinforcements to promote more insulating pore networks while maintaining acceptable mechanical performance. Overall, the findings clarify how organic and mineral fibres modify lime-based matrices and demonstrate their potential for producing thermally efficient, sustainable, and compatible mortars for building and heritage-compatible applications.

1. Introduction

Lime mortars have been employed as construction materials for millennia, playing a fundamental role in masonry and architectural heritage worldwide [1]. Today, lime-based mortars continue to receive significant attention in the restoration of heritage buildings [2]. In conservation practice, newly developed materials must be compatible with historic ones, exhibiting similar composition and properties, and their long-term effects must be carefully assessed before application [3]. Owing to its long-standing use in traditional construction, lime is a well-established material that meets these compatibility requirements. In addition, its inherent carbon dioxide (CO_2) uptake and relatively low energy demand contribute to a more sustainable approach [2,4].

Lime binders can be broadly categorized as non-hydraulic or hydraulic, according to their setting and hardening mechanisms [5]. Air lime is a non-hydraulic binder derived from high-purity limestone that hardens through carbonation, as $Ca(OH)_2$ reacts with atmospheric CO_2 in the presence of moisture to form calcium carbonate ($CaCO_3$) [6]. Air lime mortars are highly porous and permeable, offering good drying capacity and vapor exchange; however, they exhibit slow setting, low strength, poor moisture resistance, and a tendency to disintegrate under prolonged wet conditions [7,8]. Historically, these limitations were mitigated by developing hydraulic lime systems, such as the incorporation of pozzolanic materials, a technique dating back to ancient

* Correspondence to: Departamento de Química, Facultad de Ciencias, Universidad de Navarra C/ Irunlarrea, 131008 Pamplona (Navarra), Spain.
E-mail address: jalvarez@unav.es (J.I. Álvarez).

https://doi.org/10.1016/j.conbuildmat.2026.146143
Received 18 December 2025; Received in revised form 23 March 2026; Accepted 24 March 2026
0950-0618/© 2026 The Authors. Published by Elsevier Ltd. This is an open access article under the CC BY-NC license (http://creativecommons.org/licenses/by-nc/4.0/).

Table 1
Studies on basalt fibre, hemp fibre, and hemp shiv in mortars ([a]: ratios by volume of the mixture, [b]: ratios by volume of the binder, [c]: ratios by weight of the mixture, [d]: ratios by weight of the binder, [e]: ratios of binder to hemp by volume, [f]: ratios of binder to hemp by weight, *: substituted).

Study	Fibre properties			Binder type	Key findings
	Fibre type and form	Size	Ratio (%)		
Villanueva et al., 2024 [13]	Basalt fibre	12 mm	1[a]	NHL 5	- 1% basalt fibres (12 mm) improve ductility and reduce water absorption. - Manual compaction optimizes fibre dispersion.
Iucolano et al., 2013 [19]	Basalt fibre Glass fibre	n/d	1, 2[c]	NHL 3.5	- Fibres improved toughness and post-cracking behaviour. - Glass fibres (2%) showed the highest strength (2.41 MPa).
Mercuri et al., 2025 [20]	Basalt fibre	12 and 24 mm	0 −2.5[c]	Lime (70%) + OPC (30%)	- Flexural strength increases by 500–590% with 12–24 mm fibres. - Fracture energy rose by 600–1590%. - Workability decreased with fibre length and content.
Santarelli et al., 2014 [22]	Basalt continuous filament Milled basalt filament Milled basalt fibre	6.35 mm n/d n/d	3, 10[c]	NHL 3.5 NHL 3.5 + crushed bricks	- Chopped fibres (6.35 mm) improved toughness and post-peak stress capacity. - Optimal fibre content lies between 3% and 10%; excess reduces mechanical properties. - Fibres decreased capillary water absorption.
Bustos et al., 2020 [37]	Basalt fibre Glass fibre Carbon fibre	12 mm 12 mm 12 mm	0.33 −1.33[a]	NHL 5	- Mortars with fibres showed improved post-cracking behaviour. - Carbon fibres performed best, but basalt and glass fibres also enhanced toughness. - SEM confirmed good fibre-matrix bonding.
Asprone et al., 2014 [38]	Basalt fibre	4 and 5 mm	1, 2[c]	NHL 3.5	- Fibres increased porosity but enhanced ductility. - Fibre reinforced mortars showed high strain-rate sensitivity. - Fracture energy rose with strain-rate.
Yıldırım et al., 2023 [40]	Basalt fibre	12 mm	0.25, 0.5[a]	CEM I 42.5 R + Metakaolin/ Fly ash/Silica fume	- Fibres improved compressive/flexural strength at 400–600°C. - Fly ash reduced mass loss; silica fume reduced water absorption. - Fibres mitigated cracking at 800°C.
Tang et al., 2023 [41]	Basalt fibre	6 mm	0.1 −1[a]	Clay-lime mixtures (Clay: lime= 3:1, 2:1, 1:1, 1:2, 1:3)	- Best performance at 0.3% fibre dosage. - Improved shear strength and ductility in brick masonry. - Predictive formulae for shear strength validated.
Cobo Escamilla et al., 2024 [42]	Basalt fibre	6,12,18, and 24 mm	1[a]	NHL 3.5	- Flexural strength increased linearly up to 12 mm; no major gains beyond 23 mm. - Thermal conductivity rose with fibre length. - Predictive models proposed for flexural (23 mm optimum) and compressive (20 mm optimum) strength.
Guler et al., 2023 [44]	Basalt fibre	5, 10 and 24 mm, single or mixed	0.5, 1[a]	CEM I 42.5 R + volcanic ash (10%)	- Fibres reduced workability but improved freeze-thaw resistance. - Hybrid fibres slightly outperformed single fibres in compressive/flexural strength. - 5 mm fibres were most effective.
Le Troëdec et al., 2011 [24]	Hemp fibre non-treated Hemp fibre chemically treated	1–10 mm	10[b]	NHL 5	- Alkaline treatment removed amorphous compounds, improving fibre-matrix adhesion. - Treated fibres increased stress capacity by 60%. - Acoustic analysis confirmed delayed damage onset.
Avudaiappan et al., 2023 [25]	Hemp fibre	0.5, 1, and 2 cm	2 −6[d]	Hydraulic lime	- Optimal fibre length: 1 cm; ratio: 4%. - Flexural strength improved with hydration time. - EDS revealed high C, Ca, Si, Al content, enhancing bonding.
Mostefai et al., 2015 [26]	Hemp fibre Hemp shiv	1, 10, and 20 mm	1 −10[d]*	CEM II + fly ash	- Shiv increased porosity more than fibres. - Best mechanical performance: 20 mm fibres, ≤ 2% content. - Fly ash improved compressive strength (66 MPa).
Çomak et al., 2018 [27]	Hemp fibre	6, 12, and 18 mm	0 −3[a]*	CEM I 42.5 R	- 2–3% fibres (12 mm length) optimized strength. - Fibres improved flexural/splitting tensile strength. - SEM showed good fibre-cement bonding.

(*continued on next page*)

Table 1 (*continued*)

Study	Fibre properties			Binder type	Key findings
	Fibre type and form	Size	Ratio (%)		
Mahmood et al., 2024 [28]	Hemp shiv	Received, Coarse (1.33 mm), Medium (0.92 mm), Fine (0.72 mm)	1, 1:1.5, 1:2.4 [f]	Lime + slag	- Particle size reduction enhanced consistency. - Vibration compaction reduced density variation to < 3.5%. - Thermal conductivity decreased by 13% with fine shiv.
Mazhoud et al., 2016 [29]	Hemp shiv	0.43, and 0.8 mm	1:0.15 [f]	Commercial lime-based binder	- Plasters showed high porosity, hygroscopicity, and moisture buffering. - Thermal conductivity: ~0.2 W/(mK). - Optimal thickness: 6–7 cm for moisture buffering.
Evangelia et al., 2024 [35]	Hemp fibre	3 cm	1.5[a]	Lime + natural pozzolan Clay	- Fibres improved mechanical strength via stress distribution and crack bridging. - Untreated fibres enhanced self-healing via CO_2 absorption. - Hydrothermal treatment reduced porosity but did not improve self-healing.
Kesikidou et al., 2024 [36]	Hemp fibre Lavender fibre	2 cm	1[a]	Quick lime Air lime	- Hemp fibres enhanced CO_2 diffusion, improving strength. - Accelerated carbonation worked best with hot lime mixtures. - Poor adhesion with lavender fibres.
Davino et al., 2022 [39]	Hemp fibre	2 and 3 cm	0.5 −3[c]	NHL 3.5	- 1% thin braids (1 mm) improved flexural strength (+34%). - Compressive strength decreased with fibre content. - Ductility increased by 74%.
Parcesepe et al., 2021 [46]	Hemp fibre	10 −15 mm	0.2[d]	NHL 3.5	- 0.2% fibres reduced thermal conductivity by 10–11%. - Mechanical properties slightly decreased (~10–15%) due to porosity. - Aging tests showed no degradation.
Wang et al., 2021 [47]	Hemp shiv Water treated hemp shiv	2 mm	3[d]*	Pre-formulated air lime-based binder	- Water treatment removed retarding agents in shiv. - pH/conductivity of leachate predicted setting delay. - Colour not linearly related to retting degree.
Arizzi et al., 2015 [48]	Hemp hurds	2–25 mm	3:5[e]	Hydrated lime (CL90S) Hydrated lime putty (CL90S PL) NHL 3.5	- Poor matrix-hurd adhesion due to smooth hurd surface. - Delayed hardening observed; vaterite formation noted. - Suggested using fresh hurds or forced water saturation to improve hydration and adhesion.
De Bruijn et al., 2009 [49]	Hemp	Fibre:Shiv:Dust = 35:62:4	1:3[e]	Hydrated lime + NHL 5 + CEM II	- No significant strength gain from adding fibres to shiv. - Low Young's modulus limits load-bearing use. - Suggested micro silica additives for improvement.

Roman construction [9]. Unlike air lime mortars, hydraulic lime mortars set and harden in the presence of water through hydration reactions [10], which improve their mechanical strength, durability, and water resistance [6]. Lime binders may acquire hydraulic properties through different mechanisms depending on their composition and production process. Among the most common are natural hydraulic lime, air lime modified with pozzolanic materials, and ternary lime-based systems that incorporate limited amounts of cement together with pozzolans.

Natural hydraulic lime (NHL) is produced by calcining clay-bearing limestone at around 900–1100 °C, followed by slaking [6]. During calcination, the clay minerals decompose, releasing reactive SiO_2 and Al_2O_3, which react with lime (CaO) in the presence of water to form calcium silicate and aluminate hydrates (C-S-H, C-A-H). These phases impart hydraulic properties, while the free lime fraction hardens more slowly through carbonation, as $Ca(OH)_2$ reacts with atmospheric CO_2 to produce $CaCO_3$ [6,11]. NHL mortars are highly suitable for restoration works due to their compatibility with historic materials. They exhibit low shrinkage, good permeability and breathability, effective resistance to water and salts, and low stiffness that accommodates structural movements, while developing strength more rapidly than air lime mortars [6,9,11–13].

The air lime-pozzolan system represents the traditional hydraulic mortar extensively used by the Romans [9]. The pozzolanic reaction between CaO in air lime and reactive silica/alumina forms C-S-H and C-A-H hydrates, conferring hydraulicity. Nevertheless, this reaction generally proceeds more slowly than the hydration of NHL mortars and often overlaps with carbonation, with the two processes potentially interfering. The efficiency of the pozzolanic reaction depends strongly on the reactivity and composition of the pozzolan: highly amorphous siliceous or alumino-siliceous materials yield more durable mortars with improved mechanical strength [2]. Historically, natural volcanic materials and artificial pozzolans such as crushed brick and ceramic fragments were widely used [14].

Ternary lime mortars, comprising air lime, pozzolan, and cement, derive additional hydraulicity from Portland cement hydration [6,8,9]. Although pure cement mortars have caused issues in restoration due to their excessive mechanical strength, rigidity, and low water vapour permeability [6,15–17], partial substitution of air lime with limited amounts of cement, typically not exceeding 30% of the total binder content, is generally accepted in conservation practice. Such blends can enhance mechanical strength while maintaining adequate porosity and breathability [8].

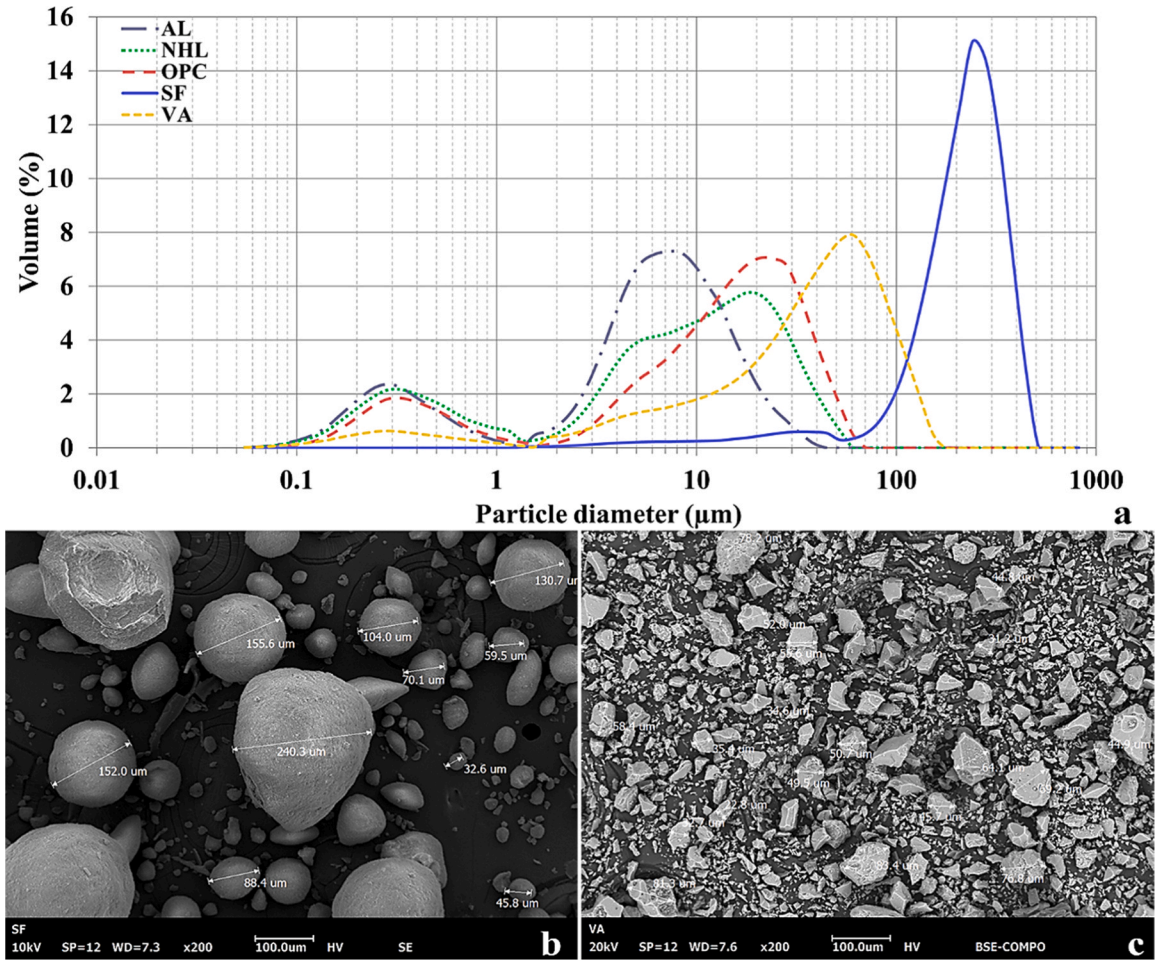

Fig. 1. (a) Particle size distribution of raw materials (AL: air lime, NHL: natural hydraulic lime, OPC: Portland cement, SF: Silica fume, VA: Volcanic ash; (b) SEM image of silica fume; (c) SEM image of volcanic ash.

Beyond hydraulicity, the performance of lime mortars has historically been improved through the addition of natural reinforcements, including natural fibres, straw, and animal hair [13,18]. This practice is now being revisited using both natural and mineral fibres, aiming to enhance durability and mechanical performance in conservation mortars [18–22]. Among natural reinforcements, hemp (*Cannabis sativa*) stands out as a low-cost, fast-growing plant that has been used in construction since prehistoric times [21,23]. Two main fractions of the hemp stem are utilised: the woody core, commonly known as hemp shiv, and the hemp fibre derived from the bast bundles of the stem. The hemp shiv, which constitutes roughly twice the volume of the fibres [23], is typically used as aggregate or filler, whereas hemp fibres are incorporated as reinforcements to improve tensile strength, mitigate cracking, and enhance thermal and acoustic behaviour [21,23–27]. Studies on hemp shiv in lime mortars have highlighted its contribution to improved hygrothermal performance and energy efficiency [28–30]. Utilizing hemp shiv also supports sustainability goals by valorising a significant by-product of hemp processing.

In parallel, mineral fibres such as basalt have been investigated for their potential to enhance lime-based mortars. Basalt fibre, produced by melting volcanic basalt stone at approximately 1500 °C and extruding it into filaments [31,32], is characterised by high tensile strength, chemical stability, and resistance to elevated temperatures, while being low-cost and possessing a long product life [19,31]. It has also been reported to have a lower environmental impact than steel and glass fibres [33,34]. Its incorporation in lime-based mortars and concretes improves flexural strength, toughness, and post-cracking behaviour through crack-bridging mechanisms [19,22], while also reducing capillary absorption and improving durability [13].

Previous studies on hemp and basalt reinforcements, summarised in Table 1, have mainly examined the effects of fibre length and dosage on performance. Overall, both reinforcements enhance flexural strength and toughness via crack-bridging mechanisms [22,35–37], though higher fibre contents commonly increase porosity and depress compressive strength in natural hydraulic lime mortars [25,37–39]. The influence of fibre reinforcement appears to be strongly dependent on the binder type. In cement-lime systems, both hemp and basalt fibres have been shown to enhance compressive strength even at relatively high dosages [20,27,40], whereas in lime-clay mortars, excessive basalt fibre content (exceeding 0.3%) can lead to strength reduction [41]. These contrasting outcomes underscore the crucial role of binder-fibre interactions in defining the mechanical response and overall performance of lime-based mortars. Nevertheless, studies involving air lime mortars remain scarce, as most research to date has focused on natural hydraulic lime [13,19,22,37,38,42,43] or cement-based systems [20,40,44]. Consequently, no studies investigated different reinforcements in different lime binder systems to compare the interactions between binder and reinforcement.

Moreover, comparative studies between mineral and natural fibres are scarce. Basalt fibres are typically compared with other mineral fibres, such as glass and carbon [19,37,43], whereas hemp fibres are assessed against other natural fibres, including lavender and sisal [36,45]. In the context of heritage restoration, the distinction between traditional natural reinforcements and more recent mineral alternatives

Table 2
Chemical composition of the raw materials (% by mass).

s	SiO_2	Al_2O_3	CaO	MgO	K_2O	Fe_2O_3	Na_2O	TiO_2	SO_3	Other Elements
Air lime	0.97	0.00	97.25	0.72	0.69	0.18	0.00	0.00	0.09	0.11
Natural hydraulic lime	16.22	2.28	77.53	1.29	0.53	0.94	0.00	0.06	0.37	0.80
Portland cement	9.61	3.33	78.30	1.26	1.35	2.70	0.00	0.19	2.11	1.14
Silica sand	95.35	2.59	0.02	0.85	0.10	0.12	0.53	0.29	0.09	0.07
Silica fume	94.07	1.89	0.66	1.13	0.79	0.29	0.41	0.02	0.46	0.30
Volcanic ash	45.77	17.13	10.22	5.53	2.57	12.62	2.40	2.56	0.10	1.12
Basalt fibre	29.81	20.16	39.48	6.01	0.49	1.24	1.24	0.82	0.40	0.74

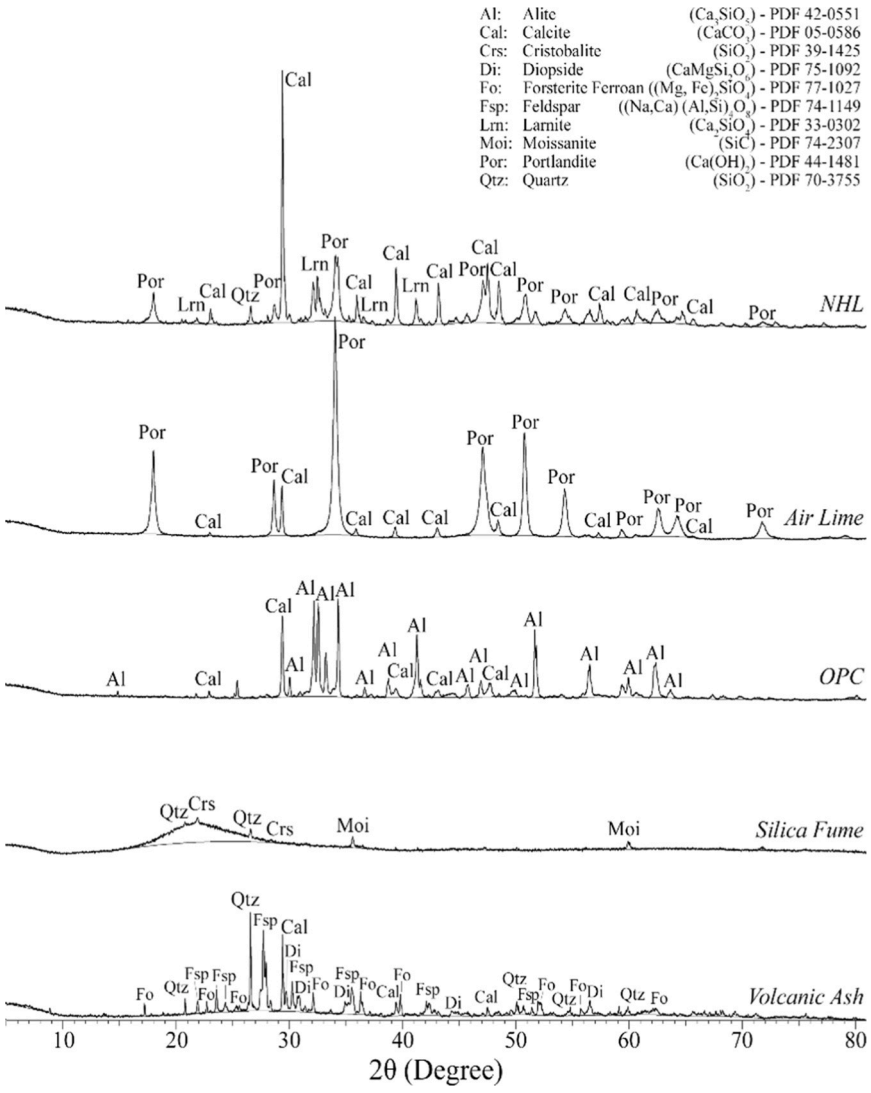

Fig. 2. XRD diffraction of raw materials (Y-axis absent as the patterns are expressed in arbitrary counts).

warrants closer evaluation. Besides, there is a gap in the literature regarding the evaluation of hemp shiv not only as an aggregate but also in terms of its potential use as a reinforcement material comparable to fibres. Addressing these gaps highlight the need to evaluate hemp shiv and basalt reinforcements under comparable conditions, particularly within the various lime-based mortar systems, commonly employed in repair works, in order to clarify their potential contribution to sustainable and heritage-compatible materials.

Accordingly, this study aims to evaluate the effects of natural and mineral reinforcements on the fresh state, physical, mechanical, and thermal properties of lime-based mortars incorporating three binder systems: natural hydraulic lime, air lime, and air lime-cement mixtures. Hemp shiv is examined beyond its conventional use as an aggregate, exploring its potential as a lightweight, thermally efficient, and sustainable reinforcement, while basalt fibre serves as a high strength, thermally stable mineral counterpart. This investigation seeks to provide a comparative understanding of how these reinforcements interact with different lime-based binders and to clarify their potential contribution to the development of sustainable materials.

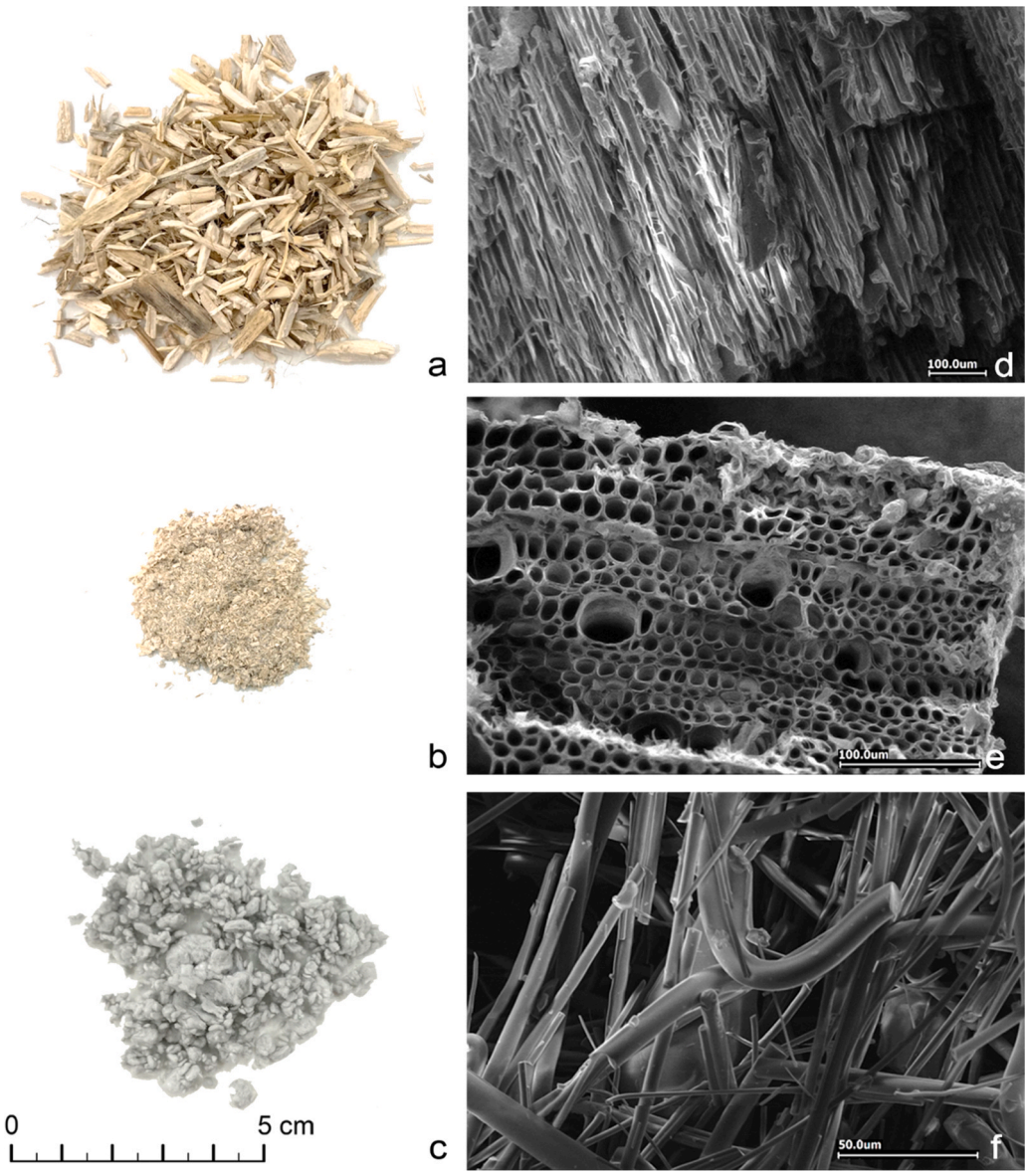

Fig. 3. Photographs of (a) raw hemp shiv, (b) ground hemp shiv, and (c) basalt fibre, along with SEM micrographs of the reinforcement materials showing (d) hemp shiv, (e) a cross-section of hemp shiv, and (f) basalt fibre.

2. Materials and methods

2.1. Characterization techniques of raw materials

The raw materials were characterized prior to mixture design using a series of analytical techniques. The chemical composition was determined by X-ray Fluorescence Spectrometry (XRF) with a Bruker S2 Puma spectrometer (Bruker Scientific Instruments, Billerica, MA, USA) equipped with a silver-anode X-ray tube. Quantitative analysis was performed using Spectra Results Manager software (Bruker AXS Spectra Elements v2.3). The mineralogical composition of the raw materials was determined using X-ray diffraction (XRD) with a Bruker D8 Advance diffractometer (Bruker AXS, Karlsruhe, Germany), employing Cu $K\alpha_1$ radiation over a 2θ range of 5–80°. Measurements were acquired with a step size of 0.03° and a counting time of 1 s per step. Data evaluations were carried out using Bruker DIFFRACplus EVA software.

The particle size distribution of the binding materials and pozzolans was analysed by laser diffraction using a Malvern Mastersizer (Malvern Panalytical Ltd., Malvern, UK). Suspensions were prepared at 1% w/w in distilled water. The particle size distribution of hemp shives was determined by sieve analysis following the RILEM test method [50], using sieves with apertures of 8 mm, 5 mm, 2 mm, 1 mm, and 0.25 mm. A 100 g sample of oven-dried shives (75 °C, to constant mass) was sieved for 3 min using a mechanical sieve shaker. Additionally, the morphology of the raw materials was examined using Scanning Electron Microscopy (COXEM EM-30N). Samples were coated with a thin gold layer using a COXEM SPT-20 ion sputter coater prior to imaging.

2.2. Materials

The particle size distribution and Scanning Electron Microscopy (SEM) images of the raw materials is illustrated in Fig. 1, and the chemical and mineralogical compositions are presented in Table 2 and Fig. 2, respectively. The lime-based mixtures were prepared using air lime, natural hydraulic lime, and Portland cement as binders. The air lime was a calcitic hydrated lime (CL90-S [10], Cal Industrial S.A., Navarra, Spain) with an average particle size of 7.27 μm (Fig. 1a). Its mineralogical composition consisted mainly of calcite and portlandite, consistent with a high CaO content. The natural hydraulic lime (NHL-5 [10], Saint-Astier, France) exhibited an average particle size of 11.77

Table 3
Composition of lime-based mortars (NHL: natural hydraulic lime, OPC: Portland cement, SP: superplasticiser).

Mixtures	NHL	Air Lime	OPC	Silica Sand	Silica Fume	Volcanic Ash	Hemp Shiv	Basalt Fibre	SP	Water/Total Solids
	(Binder: Aggregate)				*(by dry weight of binder)*					
N1	1	-	-	3	0.10	0.10	-	-	0.002	0.15
NH1	1	-	-	3	0.10	0.10	0.01	-	0.002	0.15
NH4	1	-	-	3	0.10	0.10	0.04*	-	0.105	0.15
NB1	1	-	-	3	0.10	0.10	-	0.01	0.002	0.15
NB4	1	-	-	3	0.10	0.10	-	0.04	0.003	0.15
A1	-	1	-	3	0.15	0.15	-	-	-	0.25
AH1	-	1	-	3	0.15	0.15	0.01	-	-	0.25
AH4	-	1	-	3	0.15	0.15	0.04*	-	-	0.25
AB1	-	1	-	3	0.15	0.15	-	0.01	-	0.25
AB4	-	1	-	3	0.15	0.15	-	0.04	-	0.25
CH1	-	0.85	0.15	3	0.15	0.15	0.01	-	-	0.25
CH4	-	0.85	0.15	3	0.15	0.15	0.04*	-	-	0.25
CB1	-	0.85	0.15	3	0.15	0.15	-	0.01	-	0.25
CB4	-	0.85	0.15	3	0.15	0.15	-	0.04	-	0.25

*: Grinded hemp shiv was used.

μm. Its composition was dominated by CaO and SiO_2 oxides, with calcite, portlandite, and larnite (C_2S) identified as the main crystalline phases. No presence of C_3S was identified in accordance with the low temperatures of burning of the NHL [2,48]. The Portland cement (CEM I 52.5 R [51], Cementos Portland Valderrivas S.A., Navarra, Spain) had an average particle size of 16.07 μm (Fig. 1a), with CaO and SiO_2 as the dominant oxides, accompanied by minor oxides. The XRD analysis confirmed the presence of calcite and alite (C_3S). CEN standard sand [52], consisting primarily of SiO_2 was used as the aggregate.

Two pozzolanic materials were employed: silica fume and volcanic ash. The silica fume (Fosroc Euco S.A., Bizkaia, Spain) was characterized by a high SiO_2 content, with quartz, cristobalite, and moissanite identified as the main crystalline phases, which stood out in a diffraction pattern characterized by a large amorphous halo (Table 2, Fig. 2). The volcanic ash (CTS España, Madrid, Spain) contained significant proportions of SiO_2, Al_2O_3, CaO, and Fe_2O_3. Its mineralogical composition included quartz, calcite, feldspar, forsterite ferroan, and diopside. Their average particle sizes were 224.07 μm and 43.34 μm, respectively (Fig. 1a-c).

Basalt fibre and hemp shiv were incorporated as reinforcements in the mixtures (Fig. 3a-f). The basalt fibre (CF30), supplied by Lapinus (ROCKWOOL BV, Roermond, The Netherlands), consisted mainly of SiO_2, Al_2O_3, and CaO (Table 2). The fibres had an average length of 300 ± 50 μm and an average diameter of 4.5 μm [53] (Fig. 3c, f).

Hemp shiv was also used as reinforcement, despite its more common application as an aggregate. The hemp shiv *(Cannabis sativa)*, supplied by Kanabat (La Chanvrière, France), was composed of cellulose (56%), hemicellulose (21%), and lignin (11%) according to the supplier's datasheet. Two size fractions were employed: the raw material and a portion ground in a ball mill for 1 min (Fig. 3a-b). Sieve analysis showed that the raw hemp shiv predominantly consisted of coarse particles (>8 mm: 0.2%; 8–5 mm: 5.6%; 5–2 mm: 48.3%; 2–1 mm: 34.6%; 1–0.25 mm: 11.1%; <0.25 mm: 0.1%). After 1 min of grinding, the distribution shifted toward finer particles (>8 mm: 0.0%; 8–5 mm: 0.0%; 5–2 mm: 2.0%; 2–1 mm: 32.8%; 1–0.25 mm: 56.2%; <0.25 mm: 9.0%).

To adjust mixture fluidity, a powdered superplasticiser (polycarboxylated ether derivative, MasterCast GT 205, Master Builders Solutions) was incorporated into selected mixtures as needed, ensuring a constant water-to-dry material ratio across the formulations.

2.3. Mixture design and preparation of mortars

Three binder systems were employed in this study: natural hydraulic lime (NHL), air lime, and air lime partially replaced with 15% Portland cement (Table 3). All mixtures were prepared with a binder-to-aggregate ratio of 1:3 by weight. Silica fume and volcanic ash were included as additives in equal proportions by weight, at dosages corresponding to 10% by weight of binder (bwob) in the NHL-based mixtures and 15 bwob% in the air lime mixtures. A higher pozzolan content was selected in the air lime mortars to compensate for the intrinsic hydraulicity of NHL.

Reinforcements were incorporated at two dosages corresponding to 1 bwob% and 4 bwob% of the binder, selected based on optimum levels reported in the literature [13,22,25,26]. For hemp shiv, the raw material was initially used at 1 bwob% of the binder; however, at higher contents its coarse particle size negatively affected mortar texture and workability. A preliminary study was carried out to determine the most suitable particle size [54]. Hemp shiv was ground in a ball mill, and one minute of grinding was found to yield the most favourable characteristics. Accordingly, the 4 bwob% hemp shiv dosage was introduced using the material ground for one minute.

The water-to-dry mixture ratio was kept constant within each binder system. A superplasticiser was added when required to ensure adequate workability. For the air lime mixtures, the water content was fixed at 25% of the total solids. In contrast, NHL mortars required a lower water content (15 wt%), which was supplemented with superplasticiser to achieve the desired flowability.

The mortar samples were prepared according to the mixture design presented in the Table 3. First, the dry components (binder, aggregate, pozzolanic additions, and reinforcements) were blended in a solid mixer (BL-8-CA, Lleal, S.A., Granollers, Spain) for 5 min to ensure homogeneous distribution. The predetermined amount of water and, when required, superplasticiser was then gradually added to the dry blend. Mixing was continued at low speed for 90 s using a mechanical mixer (Proeti ETI 26.0072, Proeti, Madrid, Spain).

The fresh mortar was immediately cast into moulds corresponding to the intended tests. Cylindrical specimens (30 mm diameter x 40 mm height) and disk-shaped specimens (55 mm diameter x 20 mm height) were prepared. Each mould was compacted by gentle tapping to minimise entrapped air and prevent segregation of components.

Curing conditions were selected according to the binder type: air-lime mortars, as well as ternary mortars (air lime, cement and pozzolanic material), due to their high content of air lime, were stored under controlled laboratory conditions (20 ± 2 °C, 45 ± 5% RH), whereas NHL-based mortars were cured in a high-humidity curing chamber (20 ± 2 °C, 95 ± 5% RH). After 7 days, all specimens were demoulded and maintained under the same environmental conditions until testing. Analyses were performed after 7, 28, 91, and 182 days of curing.

2.4. Experimental tests

The prepared mortar mixtures were subjected to several experimental tests. A detailed overview of the experimental procedures for all

Table 4
Results of fresh state analyses (SP: content of superplasticiser), and open porosity, apparent density and water absorption coefficient obtained by hydrostatic tests, and bulk density and average pore diameter obtained by MIP.

Mixtures	SP (bwob %)	Slump Values (mm)	Water Retention (%)	Open porosity (%)	Bulk density (g/mL)	Water Absorption Coefficient (kg/m^2.min$^{0.5}$)	Average Pore Diameter (μm)
N1	0.20	180.0	94.88	22.30	1.88	0.31	0.05
NH1	0.20	168.0	90.65	23.26	1.84	0.39	0.06
NH4	1.05	173.0	96.73	40.28	1.59	0.17	0.05
NB1	0.20	174.0	90.51	22.80	1.92	0.39	0.05
NB4	0.30	175.0	94.44	23.24	1.82	0.43	0.05
A1	-	185.0	94.24	31.45	1.50	3.43	0.37
AH1	-	187.5	91.83	31.92	1.73	3.12	0.22
AH4	-	173.0	95.68	35.61	1.57	3.06	0.34
AB1	-	190.0	93.39	30.46	1.72	3.45	0.23
AB4	-	193.0	95.16	31.89	1.48	3.58	0.50
CH1	-	192.5	91.66	33.20	1.65	4.40	0.25
CH4	-	185.0	94.57	34.75	1.45	3.04	0.35
CB1	-	198.0	91.16	31.59	1.77	4.01	0.21
CB4	-	197.0	90.78	34.15	1.67	4.52	0.21

measurements performed in this study is provided in the supplementary material (Table S1).

2.4.1. Fresh state tests

The fresh state properties of mixtures were assessed through flowability and water retentivity tests. Flowability was evaluated using the flow table method in accordance with the UNE-EN 1015–3 [55]. Water retention capacity, reflecting the ability of the mixture to retain mixing water under suction forces, was determined following UNE 83816 [56].

2.4.2. Physical and microstructural characterization

The physical and microstructural characteristics of the mortars were assessed through measurements of open porosity, water capillary absorption, pore size distribution, complemented by SEM observations. Open porosity was determined using the water saturation method [57], while water absorption due to capillarity was measured according to UNE-EN 15801 [58]. Both tests were conducted after 182 days of curing.

Pore size distribution and bulk density was analysed by mercury intrusion porosimetry (MIP) at 91 days of curing using a Micromeritics AutoPore IV 9500 (Micromeritics Instrument Corp., Norcross, GA, USA), operating over a pressure range of 0.0015–207 MPa.

Microstructural observations were performed using scanning electron microscopy (SEM) with a COXEM EM-30N microscope (COXEM Co. Ltd., Daejeon, South Korea) equipped with an energy-dispersive X-ray spectroscopy (EDS) detector (Bruker Corporation, Billerica, MA, USA). The samples were mounted on aluminium stubs with carbon tape and coated with a thin layer of gold using a COXEM SPT-20 ion sputter coater. Imaging was carried out under high-vacuum conditions using both secondary electron (SE) and backscattered electron detectors (BSE).

2.4.3. Compressive strength tests

Compressive strength was measured after 7, 28, 91, and 182 days of curing. Three cylindrical specimens were tested at each curing age to ensure statistical reliability. Tests were performed using a Frank/Controls 81565 press coupled with a Proeti ETI 26.0052 compression device. Loading was applied at a controlled rate of 20–50 N/s, with total loading time maintained between 30 and 90 s.

2.4.4. Thermogravimetric analyses

Hydration and carbonation processes were evaluated through thermogravimetric analyses (TGA). Samples were placed in 90 μL alumina pans and analysed using an SDT650 (TA Instruments, New Castle, DE, USA). Data were processed with TRIOS software from TA Instruments. A controlled heating rate of 20 °C/min was applied from 35 °C to 1100 °C under a 50 mL/min nitrogen environment, with a flow of nitrogen purge gas flow of 100 mL/min.

2.4.5. Thermal conductivity measurements

Thermal conductivity was measured on disk-shaped specimens using a FOX50 Heat Flow Meter (TA Instruments). The instrument uses two parallel plates, each independently temperature-controlled by Peltier cells, maintaining a constant temperature difference of 10 °C. This configuration establishes a stable thermal gradient, enabling determination of thermal conductivity at mean temperatures of 5, 15, 25, and 35 °C. These temperatures were selected to represent both seasonal variations and a range of climatic conditions. In this context, 5 °C reflects colder climate or winter conditions, 15–25 °C correspond to temperate or spring/autumn conditions, and 35 °C represents warmer or summer conditions. Two specimens per mixture were tested to allow cross-validation and minimise experimental error.

2.4.6. Weighting-scoring method for the performance assessment

A weighting–property methodology [59] was used to evaluate the performance of the lime-based mortars under two usage scenarios: (i) use as a bedding mortar and (ii) use as a rendering material. For this assessment, four performance indicators (compressive strength, thermal conductivity, water absorption coefficient, and open porosity) were combined using different weighting scores depending on the application scenario.

Firstly, the results were normalised using the min–max scaling method according to Eq. (1) and expressed on a scale from 0 (lowest performance) to 1 (highest performance) [60]. For indicators in which lower values correspond to better performance, the normalised values were inverted by subtracting them from 1.

$$S_0 = \frac{I_x - I_{\min}}{I_{\max} - I_{\min}} \quad (1)$$

Where S_0 is the normalised score of the mortar, $I_{\min}$ and $I_{\max}$ are the minimum and maximum values of the indicator across all mixtures, and I_x is the result for sample x. The normalised scores were multiplied by weighting scores decided according to the priority for each scenario.

3. Results and discussion

3.1. Fresh state analyses

The fresh state behaviour of the mixtures was evaluated through fluidity and water retention measurements, and the results are presented in Table 4. Binder type was the main factor influencing the mixture consistency. The water-to-dry material ratio was adjusted according to binder type to obtain suitable slump values. Mixtures containing natural

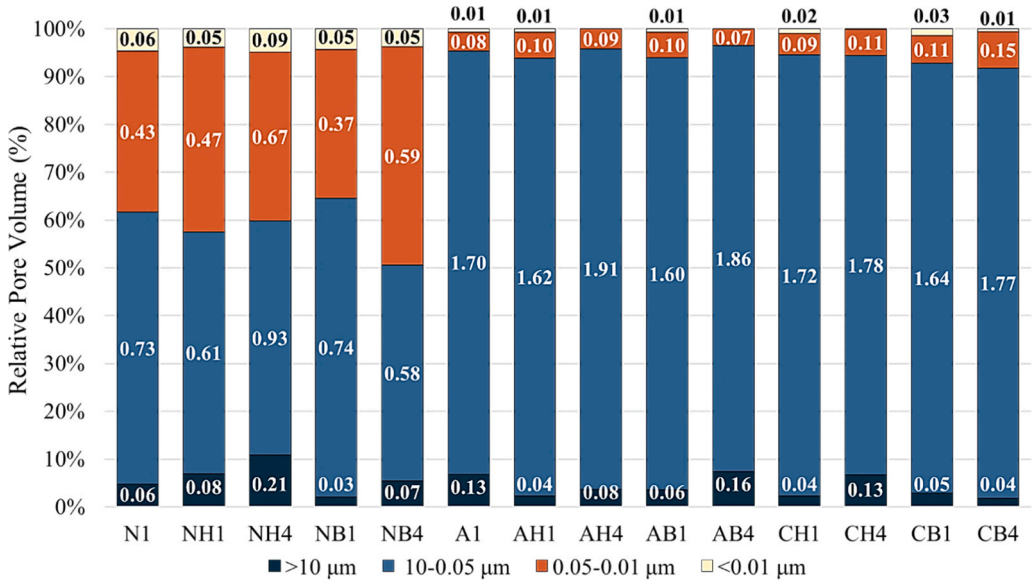

Fig. 4. Relative distribution of air voids (>10 µm), large capillary pores (10–0.05 µm), medium capillary pores (0.05–0.01 µm), and gel pores (<0.01 µm). The specific pore volume of each size range (mL/g) is shown within corresponding bar segments.

hydraulic lime (NHL) required less water (15 wt%) than those based on air lime (25 wt%). Partial substitution of air lime with Portland cement (OPC) further increased slump values. The higher water demand and lower slump values observed in air lime mixtures (without OPC) can be attributed to the smaller particle size of air lime compared with NHL and OPC (Fig. 1a), which yields a higher specific surface area [17,61].

The effects of hemp shiv and basalt fibre were also evident (Table 4). Hemp shiv incorporation generally reduced slump, with the reduction becoming more pronounced at the higher dosage (4 bwob%). In NHL-based mortars, NH1 exhibited a 7% slump reduction relative to the reference mixture N1. At 4 bwob% hemp shiv, mixture NH4 required a higher superplasticiser dosage to maintain workable consistency. In air lime mortars, the addition of 1 bwob% hemp shiv had a minimal effect; AH1 even showed a slight increase in slump (187.5 mm) compared with A1 (185 mm). However, at 4 bwob%, fluidity decreased by 7.5% in the air lime system and by 3.9% in the ternary system compared to their respective 1 bwob% mixtures. This behaviour is attributed to high water absorption of hemp shiv and its barrier effect, which restricts mortar flow [26,62].

In contrast, basalt fibre showed only a limited influence on consistency. A slight reduction in slump (approximately 3%) was observed at 1 bwob% in the NHL-based mortars. In contrast, the same dosage in air lime-based mortars led to an increase in slump, by about 3% in AB1 and 7% in CB1. At 4 bwob%, basalt fibre did not induce a consistent trend, and its overall impact remained minor compared with hemp shiv.

The water retention capacity of all mixtures exceeded 90% (Table 4). Variations were mainly associated with the type and dosage of reinforcement. Across all binder systems, the incorporation of 1 bwob% reinforcement caused a slight reduction in water retention. At 4 bwob%, retention increased, particularly in mixtures containing hemp shiv. The only exception occurred in the ternary mortars with basalt fibre, where higher fibre contents resulted in a decrease. The highest water retention value was observed in NH4 (96.73%), attributed to the combined effect of the elevated hemp shiv content and the increased superplasticiser dosage. Superplasticisers and viscosity-modifying agents are known to retain water within the mixture for longer, resulting in increased water retention [63].

3.2. Physical and microstructural characterization

3.2.1. Open porosity and bulk density

Open porosity values revealed clear trends influenced by both the binder type and the presence of reinforcements (Table 4). In general, NHL mortars exhibited the lowest open porosity (22.30–23.26%, except for NH4) whereas air lime mortars (30.46–35.61%) and ternary mortars (31.59–34.75%) showed markedly higher porosity.

As expected, the introduction of fibrous reinforcements tended to increase porosity, primarily due to the formation of interfacial transition zones and additional air voids. The effect of hemp shiv was evident in all binder systems, though modest at the lower dosage: AH1 and NH1 displayed porosity increases of 1.5% and 4.3%, respectively, compared to their reference mortars. In the ternary system (CH1), the combined presence of cement and hemp shiv resulted in a slightly higher porosity increase than in AH1.

At the higher dosage (4 bwob%), the impact of hemp shiv became more pronounced. The porosity of AH4 increased to 35.61%, representing a 13% rise relative to A1, whereas NH4 exhibited an exceptionally high porosity of 40.28%, corresponding to an 81% increase compared to N1. The substantial rise is attributed to the finely ground hemp shiv, which generated a large volume of macroscopic air voids during mixing. The increase observed in NH4 may also be attributed to its high superplasticiser content. A similar trend associated with superplasticiser addition was reported by Silva et al. (2019) [64]. By contrast, the influence of basalt fibre on porosity was more limited. While porosity tended to increase with higher fibre contents, the magnitude of change remained considerably lower that the observed for hemp shiv. This behaviour may be explained by the much smaller dimensions of basalt fibres, which could lead to narrower interfacial gaps and therefore a lower contribution to the overall pore volume in the matrix [42].

The density values were found to be consistent with the open porosity results (Table 4). The NHL-based samples exhibited the highest bulk density values (1.59–1.92 g/mL), indicating a denser structure, followed by air lime-based mortars (1.48–1.73 g/mL) and ternary mortars (1.45–1.77 g/mL). The incorporation of reinforcement at low dosages led to an increase in bulk density up to 2% in NHL-based mortars, and 15% in air lime-based mortars, despite the observed increase in porosity compared to the reference samples. At higher reinforcement contents, however, a reduction in density was observed. This decrease can be associated with the combined effect of increased

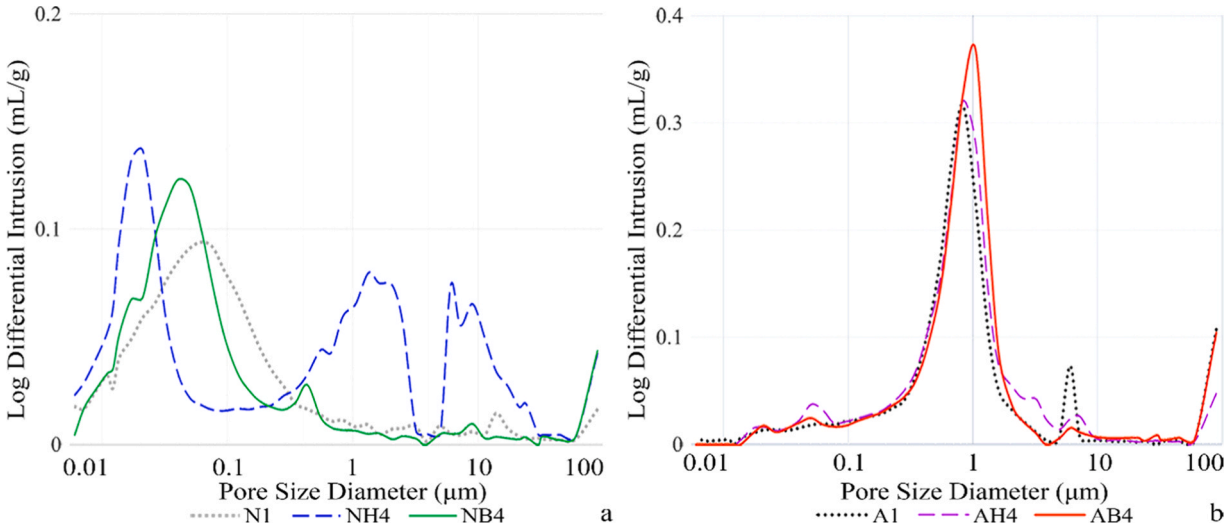

Fig. 5. Comparative pore size distributions of (a) natural hydraulic lime mortars and (b) air lime mortars at 91 days of curing. The graphs represent the control mortar, without reinforcement, and the samples with hemp shiv and basalt fibre.

porosity and the intrinsically low density of the fibres. Although the comparison between basalt fibre and hemp shiv does not show a strictly uniform trend across all mixtures, hemp shiv generally resulted in a more pronounced reduction in bulk density.

3.2.2. *Pore size distribution*

The pore size distribution within mortar matrices is influenced by the mixing process, the constituent materials, and the chemical reactions occurring during curing. Air voids (>10 μm) originate mainly from entrapped air during mixing and from shrinkage-induced discontinuities. Large (10–0.05 μm) and medium (0.05–0.01 μm) capillary pores are governed by the water-to-binder and binder-to-aggregate ratios [65,66]. These pores control moisture transport: smaller capillary pores generate higher suction but slower liquid flow, whereas larger capillary pores generate faster moisture movement with weaker capillary forces [67]. Pores larger than 0.01 μm also contribute significantly to the mechanical behaviour of mortars [65]. Gel pores (<0.01 μm), by contrast, are associated with hydration and pozzolanic reactions and are commonly found in mortars containing natural hydraulic lime [65,66].

The results of mercury intrusion porosimetry (MIP) were given in Table 4 and Fig. 4, and in the supplementary material, Figure S1 and Figure S2. Pore size distribution determined provides insight into the microstructural differences arising from binder type and reinforcement. Mortars prepared with natural hydraulic lime displayed a considerably finer pore network, with average pore diameters of 0.05–0.06 μm. In contrast, air lime mortars exhibited average pore sizes of 0.22–0.50 μm, while ternary mortars ranged from 0.21 to 0.35 (Table 4). The dominant pore-size peak for NHL mortars occurred between 0.01 and 0.1 μm, whereas in air lime mortars it shifted to the 0.5–1 μm range (Supplementary Material, Figure S1 and Figure S2), consistent with typical lime-based systems [65,68]. Additionally, NHL mortars contained a measurable proportion of gel pores (3–5% of total pore volume), while these were nearly absent in air lime mixtures (Fig. 4). These differences reflect the distinct reaction mechanisms: hydration reactions in NHL mortars produce C-S-H and other hydrates that fill capillary voids and generate gel pores, resulting in reduced overall porosity and finer pore structures [66,69,70].

Reinforcement additions exerted a secondary but discernible influence on pore size characteristics. In NHL-based mortars, hemp shiv increased the proportion of air voids, particularly in NH4, which showed the highest hemp content (Fig. 4, Fig. 5a). Although the average pore diameter remained nearly unchanged, the elevated air-void fraction aligns with the substantial increase in open porosity observed for NH4. In contrast, air lime mortars containing hemp shiv exhibited a reduction in air voids and a corresponding decrease in average pore size, especially in AH1 and CH1 with 1 bwob% hemp addition (Table 4). This suggests that a small amount of hemp shiv may promote a more compact internal structure in these systems.

The effect of basalt fibre on pore structure was comparatively minor. Only an increase in medium capillary pores (0.05–0.01 μm) was observed in NB4 accounting for 46%, with similar but less pronounced shifts in AB1, CB1, and CB4 (Supplementary Material, Figure S2). The limited changes indicate that basalt fibres do not significantly disrupt the paste matrix or the formation of air voids.

Overall, the results indicate that hemp shiv had a more pronounced influence on pore morphology than basalt fibre, mainly by altering the distribution and connectivity of air voids rather than refining the capillary pore network (Fig. 5a-b).

3.2.3. *Capillary water absorption*

The water absorption coefficients of the mortars are presented in Table 4. NHL-based mortars exhibited the lowest water absorption coefficients, ranging from 0.17 to 0.43 kg/m^2·min$^{0.5}$. Although these samples mainly consist of medium and large capillary pores, which govern water transport within the material structure, the overall dense microstructure and low total porosity of NHL mortars reduced capillary absorption. In contrast, the higher open porosity and the predominance of large capillary pores, as evidenced by the MIP results, in air-lime and ternary mortars resulted in markedly higher absorption coefficients, ranging from 3.06 to 3.58 kg/m^2·min$^{0.5}$ and 3.04–4.52 kg/m^2·min$^{0.5}$, respectively.

Previous studies have reported that hemp fibres tend to increase water absorption [27,36], whereas basalt fibres may reduce it by limiting the formation of cracks and preferential capillary pathways [13,40,42]. However, in the present study, hemp shiv produced the opposite trend: mortars containing hemp shiv generally showed lower water absorption than their respective reference mixtures (Table 4). Although NH1 exhibited slightly higher initial suction (0.39 kg/m^2·min$^{0.5}$) than N1 (0.31 kg/m^2·min$^{0.5}$), NH4 showed a pronounced reduction, with a coefficient of 0.17 kg/m^2·min$^{0.5}$. This decrease may be partly attributed to the increased dosage of superplasticiser in NH4, as Silva et al. [64] noted that superplasticisers can reduce capillary absorption in lime mortars. The excess of superplasticizer may cause partial hydrophobic effects at the pore wall interface that would reduce water–solid affinity, thereby limiting effective capillary suction even in the presence of larger pores.

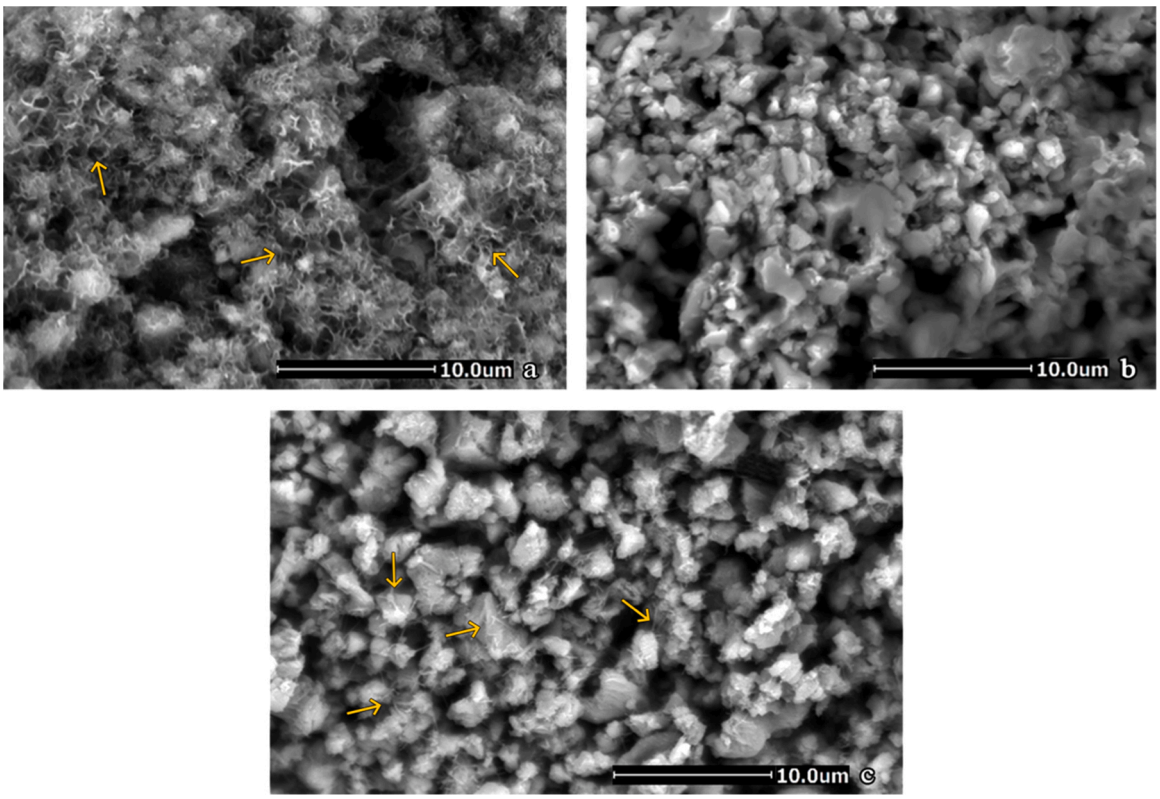

Fig. 6. SEM-BSE images showing the binder matrix: (a) N1, arrows indicate a web-like structure; (b) A1; (c) CH4, arrows indicate needle-like ettringite crystals.

In the air lime mortars, both mixtures containing hemp shiv exhibited progressively lower absorption coefficients than the reference (Table 4), confirming their reduced capillary action. Moreover, the increased hemp content in AH4 further decreased the water absorption coefficient for 11%, following a trend similar to that observed in the NHL mortars. Ternary mortars generally showed higher capillary absorption than air lime mortars, consistent with their higher total porosity and the predominance of capillary pores revealed by MIP, particularly within the larger capillary range. Nevertheless, CH4 exhibited a lower water absorption coefficient (3.04 $kg/m^2.min^{0.5}$), which may be attributed to the formation of additional air voids, as indicated by the MIP results, resulting from interactions between the binder and hemp shiv. These air voids could cut off the capillary network, thus decreasing the water absorption [71,72].

For basalt fibre–reinforced mortars, the behaviour differed from trends reported in the literature [13,40,42]. Although the overall influence was limited, a slight increase in water absorption was observed with increasing fibre content. In NHL-based mortars, the increase observed in NB1 was 28% and in NB4 was 42%, which can be associated with an increase in capillary pores compared to N1. In particular, NB4 shows a shift toward medium capillary pores, which may enhance capillary suction. In the air lime and ternary systems, already characterised by high porosity and coarse, interconnected capillary networks, the incorporation of basalt fibres further increased the absorption coefficient, likely by enhancing pore connectivity and enlarging the effective capillary pathways. AB1, AB4, CB1, and CB4 all exhibited higher values than their reference mixtures (Table 4). This suggests that basalt fibres were unable to counteract the strong capillary suction inherent to these binders and may have introduced additional interfaces or discontinuities. Notably, CB4 exhibited the highest absorption coefficient (4.52 $kg/m^2{\cdot}min^{0.5}$) and also presented the highest proportion of capillary pores within the 0.01–10 μm range, accounting for approximately 97% of its total pore volume according to MIP results. This predominance of capillary-sized pores can explain its enhanced capillary suction behaviour.

3.2.4. *Microstructural assessment*

The microstructural characteristics of samples on 91 days of curing were examined using scanning electron microscopy (SEM), which allowed detailed observation of the matrix–reinforcement interface and the morphological features governing their interaction. The morphology of the mortar matrix differed according to the binder type, as shown in the SEM images (Fig. 6). NHL mortars exhibited a denser and more homogeneous microstructure, characterized by a web-like network formed by hydration products (Fig. 6a). In contrast, the air lime and ternary mortars showed a more porous matrix with noticeable discontinuities (Fig. 6b-c). These matrices consisted mainly of carbonation products, and needle-like ettringite crystals were additionally identified in the ternary mortar (Fig. 6c).

Building on these observations, the addition of reinforcement materials introduced further microstructural changes, most notably at the matrix-shiv interface. As shown in Fig. 7, the weak adhesion between the shiv particles and the binder resulted in the formation of interfacial gaps, which consequently increased the overall porosity of the mortars. Larger hemp particles intensified this effect, producing wider gaps that in some regions exceeded 100 μm (Fig. 7a-d). In the samples containing finely ground hemp shiv (NH4, AH4, and CH4), the smaller particle size increased the contact area with the matrix, leading to noticeably narrower gaps (Fig. 7e). The chemical composition of hemp, comprising cellulose, hemicellulose, and lignin, governs its surface morphology and contributes to the development of a heterogeneous interface with lime, influencing the overall quality of the bond [24]. Arizzi et al. (2015) [48] further reported that the poor adhesion between hemp and the lime matrix is linked to the high-water absorption of the shiv, which restricts the deposition of lime particles at the interface. Their study also examined the penetration of the lime matrix into the shiv particles and concluded that, due to this weak adhesion, lime particles were unable to reach the interior of the shives.

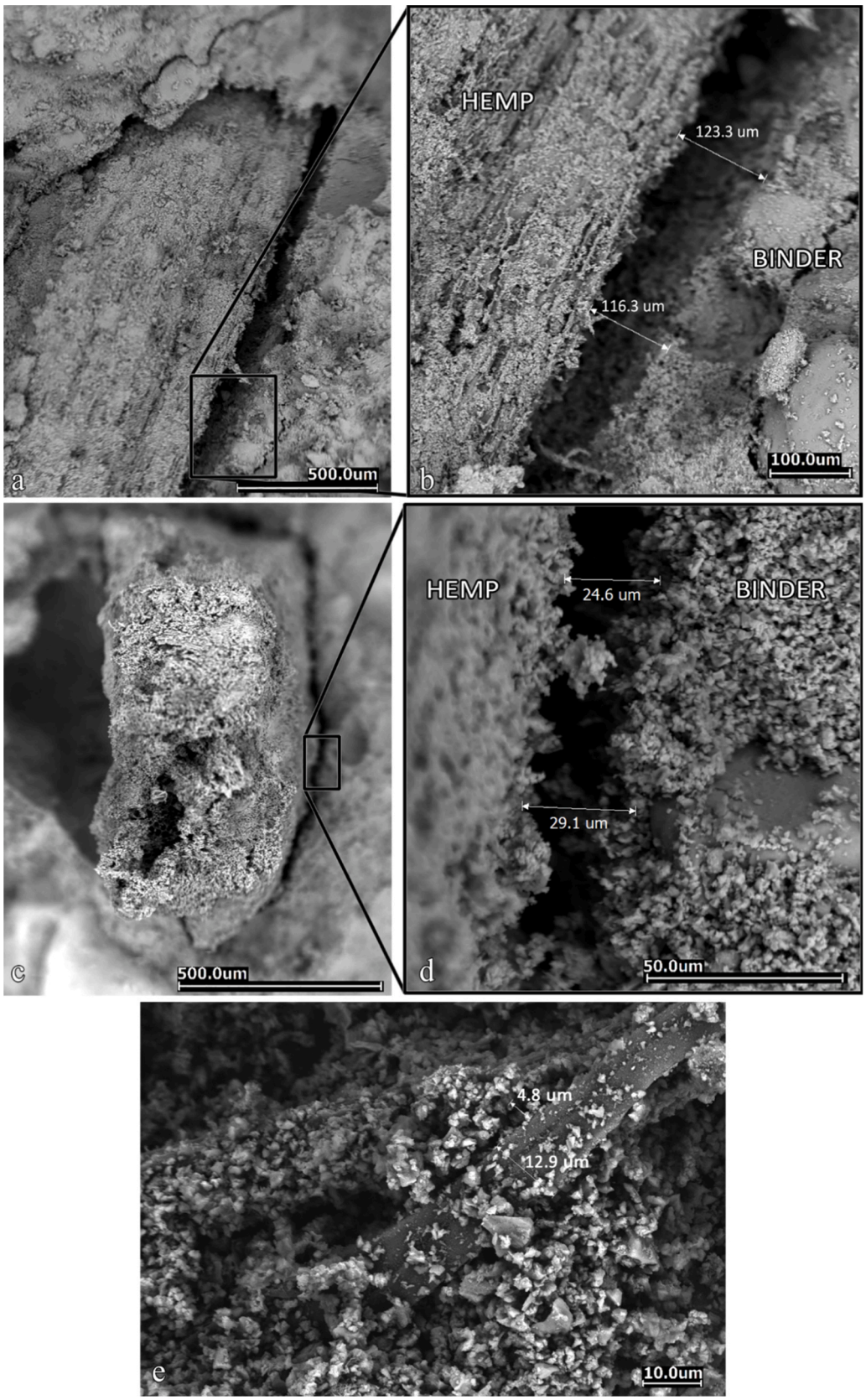

Fig. 7. SEM-BSE images of mortars reinforced with hemp shiv: (a) NH1; (b) enlarged view of the squared region in NH1; (c) AH1; (d) enlarged view of the squared region in AH1; (e) AH4.

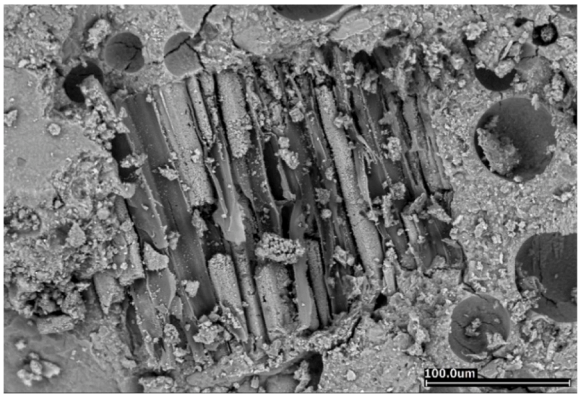

Fig. 8. SEM-BSE image of NH4, showing well-bonding between binder and hemp shiv.

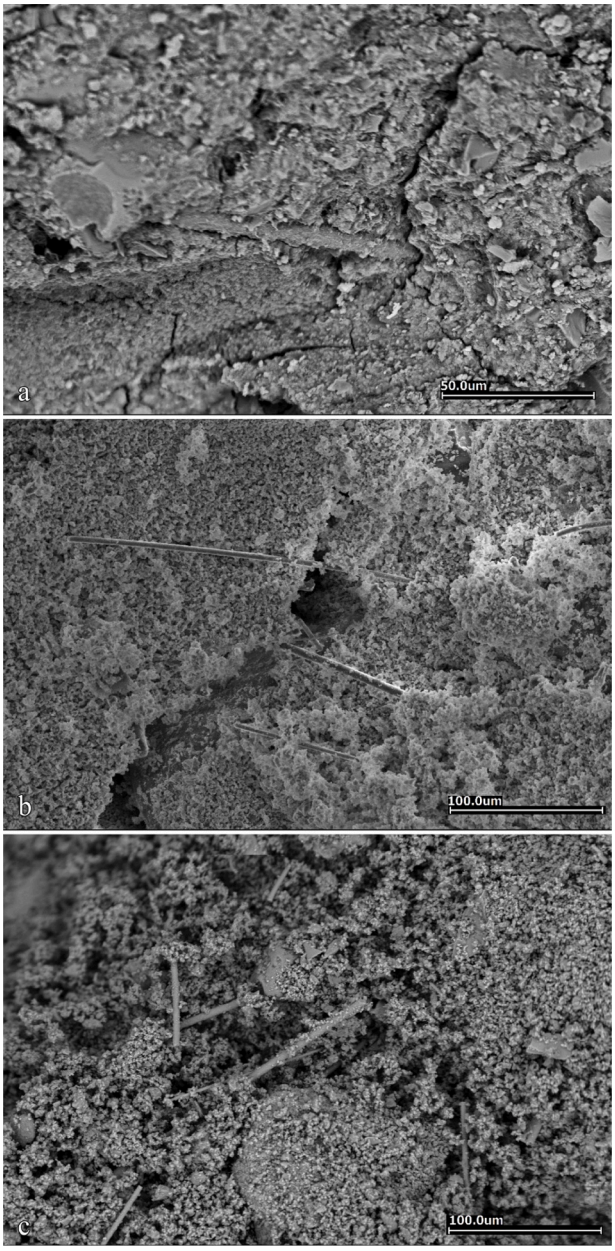

Fig. 9. SEM-BSE images of mortars reinforced with basalt fibre: (a) NB4; (b) AB4; (c) CB4.

In this study, consistent with previous findings, the lime matrix did not fully penetrate the porous structure of the raw hemp shiv regardless of the binder type; however, grinding the shiv enhanced matrix penetration. An exception was observed in NH4, where strong bonding between the hemp particles and the NHL matrix was clearly visible, and penetration of the binder into the internal channels of the shives was evident (Fig. 8). The higher superplasticiser content (1.05 bwob%) may explain this behaviour, as the same effect was not observed in NH1. Fig. 8 also revealed the presence of numerous air voids in NH4, consistent with its high porosity (40.28%) and pore size distribution results (Table 4, Fig. 4). The large voids, dispersed within the dense binder matrix, may be associated with: i) the presence of cellulose-based components, which are expected to be more abundant in samples with higher hemp content, such as NH4. These components may exhibit a mild tensioactive behaviour, contributing to the stabilisation of entrapped air during mixing. A comparable air-entrainment phenomenon has been reported for cellulose ethers [73]. ii) The combined increase in hemp shiv content and superplasticiser dosage may further favour air retention in the NH4 mixture. Hemp shives possess a porous internal structure with longitudinal channels (Fig. 3e) that can trap and physically retain air, while the superplasticizer, due to its bipolar nature, can stabilize air bubbles during mixing. However, the individual contributions of these factors cannot be clearly distinguished.

Based on the examination of multiple micrographs taken from different regions of the samples, no noticeable fibre agglomeration was observed. Fig. 9 illustrate a generally homogeneous fibre distribution within the matrix. However, the basalt fibres did not appear to be fully embedded within the matrix, especially in air lime and ternary mortars, suggesting a relatively weak fibre–matrix interfacial bond. In NHL mortars, although fibres were more attached to the binder, microcracks were still noticeable in the interfacial zone (Fig. 9a). Although the basalt fibres exhibited limited interfacial bonding, especially in air lime and ternary mortars, the bridging mechanism was clearly visible (Fig. 9b-c). As described by Santarelli et al. (2014) [22], partial debonding allowed the fibres to span across microcracks and generate crack-closure forces, thereby contributing to crack arrest and improved post-cracking resistance.

3.3. *Compressive strength*

The compressive strength results at 7, 28, 91, and 182 days of curing are presented in Fig. 10 and Fig. 11. NHL-based mortars exhibited the highest mechanical performance among all binder systems, confirming the hydraulic behaviour and early strength gain typically associated with this binder (Fig. 10). The denser microstructure observed in the bulk density measurements and SEM images contributed to the improvement of compressive strength in the NHL-based mortars. In addition, the higher water-to-solid ratio used in air lime and ternary mortars (25 wt%) compared to NHL-based mixtures (15 wt%) might contribute to their lower strength development, as increased water content generally promotes higher initial porosity after evaporation and lower compressive strength.

The incorporation of hemp shiv resulted in a noticeable reduction in early-age compressive strength, primarily due to increased porosity and limited interfacial bonding between the organic particles and the lime matrix observed in SEM (Fig. 7). However, by 91 days, both NH1 (9.2 MPa) and NH4 (9.0 MPa) surpassed the strength of the reference mortar (8.4 MPa). This improvement was not sustained at later ages: NH4 displayed a reduction in strength at 182 days (7.0 MPa), likely reflecting its higher porosity and the weaker adhesion between the shiv and the matrix. The same behaviour was reported by Davino et al. (2022) [39]. It was observed that NHL mortars reinforced with hemp braids exhibited reduced compressive strength with increasing dosage, decreasing from 4.6 MPa to 3.4 MPa at 28 days.

The mechanical performance of basalt fibre-reinforced NHL mortars varied with fibre content. NB1 exhibited strength values similar to the

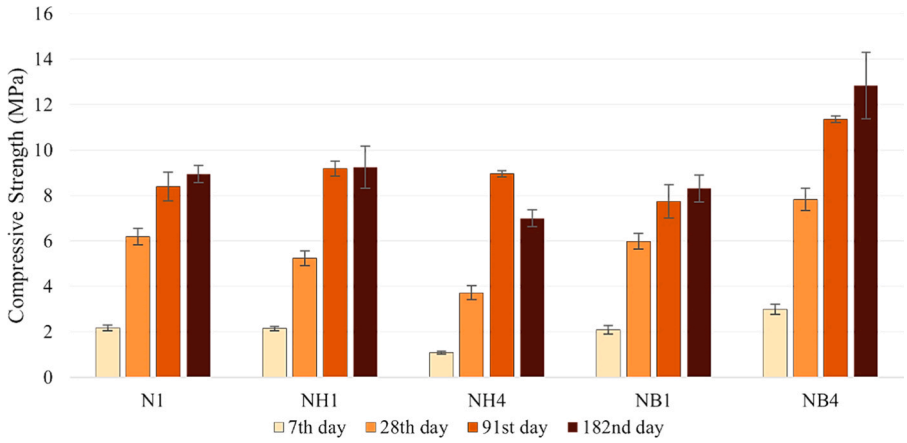

Fig. 10. Compressive strength of NHL-based mortars. Error bars indicate standard deviation.

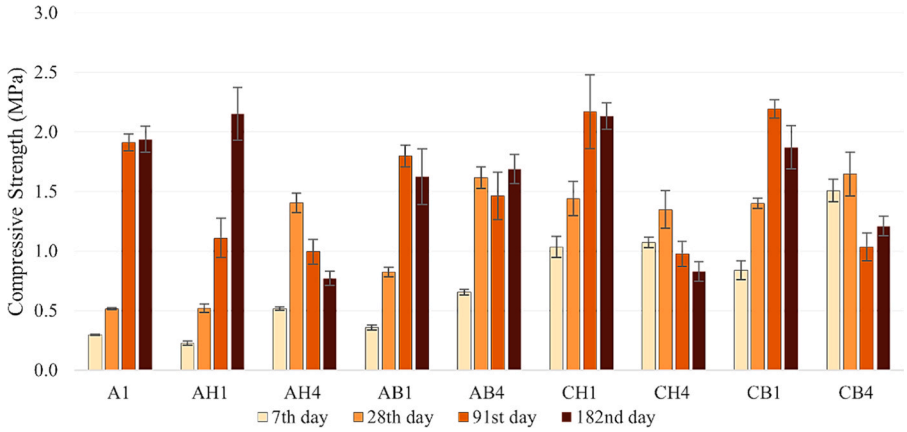

Fig. 11. Compressive strength of air lime-based and ternary mortars. Error bars indicate standard deviation.

reference mixture at all curing ages, whereas NB4 showed a continuous increase in strength, reaching 12.8 MPa at 182 days, the highest value recorded across all mixtures (Fig. 10). This improvement is attributed to the crack-bridging capability of basalt fibres, which helps to redistribute stresses and delay crack propagation [22]; this mechanism was also clearly observed in the SEM images, where partially debonded fibres were seen spanning microcracks and contributing to crack arrest. The previously discussed microstructural results also support this behaviour: basalt fibre addition in NHL mortars reduced the proportion of medium and large capillary pores, contributing to a denser matrix and enhanced long-term load-bearing capacity. Similar strength improvements in basalt fibre-reinforced NHL mortars have been reported in previous studies [13,40,42].

Moreover, the addition of superplasticiser was reported to have a positive effect on compressive strength [64,74]. In our study, among the NHL-based mortars, the superplasticiser dosage was kept within a narrow range (0.2 −0.3 bwob%), except for NHL4 (1.05 bwob%). Consequently, its effect cannot be observed clearly. Also, the strength reduction observed in NHL4 was more consistently explained by higher hemp content and increased porosity than by the superplasticiser.

By contrast, air lime-based mortars exhibited substantially lower compressive strength, not exceeding 2 MPa after 182 days (Fig. 11). Their limited mechanical development is attributable to the slow carbonation process and the absence of hydraulic phases; in fact, carbonation under ambient environmental conditions, where carbon dioxide concentrations are relatively low, is a very slow process that can take several years to progress significantly [2]. The addition of hemp shiv did not enhance compressive strength. Although AH4 showed better early-age performance than A1 and AH1, reaching nearly three times higher strength at 28 days. Its strength declined after 28 days from 1.40 MPa to 0.77 MPa until 182 days. This reduction can be attributed to the combined effects of increased porosity and the development of a coarser pore structure. Only a minor late-age improvement was observed for AH1, which reached 2.2 MPa at 182 days, slightly higher than A1 (1.9 MPa). For ternary lime mortars, the low dosage mixture CH1 showed steady growth up to 91 days (2.2 MPa), whereas CH4 declined after early ages, reaching only 0.83 MPa at 182 days. Even though the use of larger shives at lower dosages was observed in the SEM images to create wider interfacial gaps, the incorporation of higher amounts of ground shives led to a greater reduction in compressive strength. This reduction is associated with the lower density values of the samples containing 4 bwob% shives compared to those with 1 bwob %. Evangelia et al. (2024) [35] reported more pronounced strength development in lime–pozzolan mortars reinforced with hemp fibre, reaching approximately 10 MPa after 180 days. In contrast, Kesikidou et al. (2024) [36] reported lower strength values, comparable to those obtained in the present study, with air lime-based mortars reinforced with hemp fibre reaching 1.54 MPa at 180 days.

Basalt fibre improved the early-age behaviour of air lime and ternary mortars, particularly at 7 and 28 days, where the influence of fibre dosage became evident. At 28 days, AB4 reached 1.6 MPa, outperforming AB1 (0.8 MPa) and the reference A1 (0.5 MPa). However, the long-term development remained limited, and both AB1 and AB4 showed lower strength than the reference mortar beyond 91 days. CB1 increased to 2.2 MPa at 91 days and then decreased to 1.87 MPa at 182 days. In contrast, CB4 showed improved early-age performance

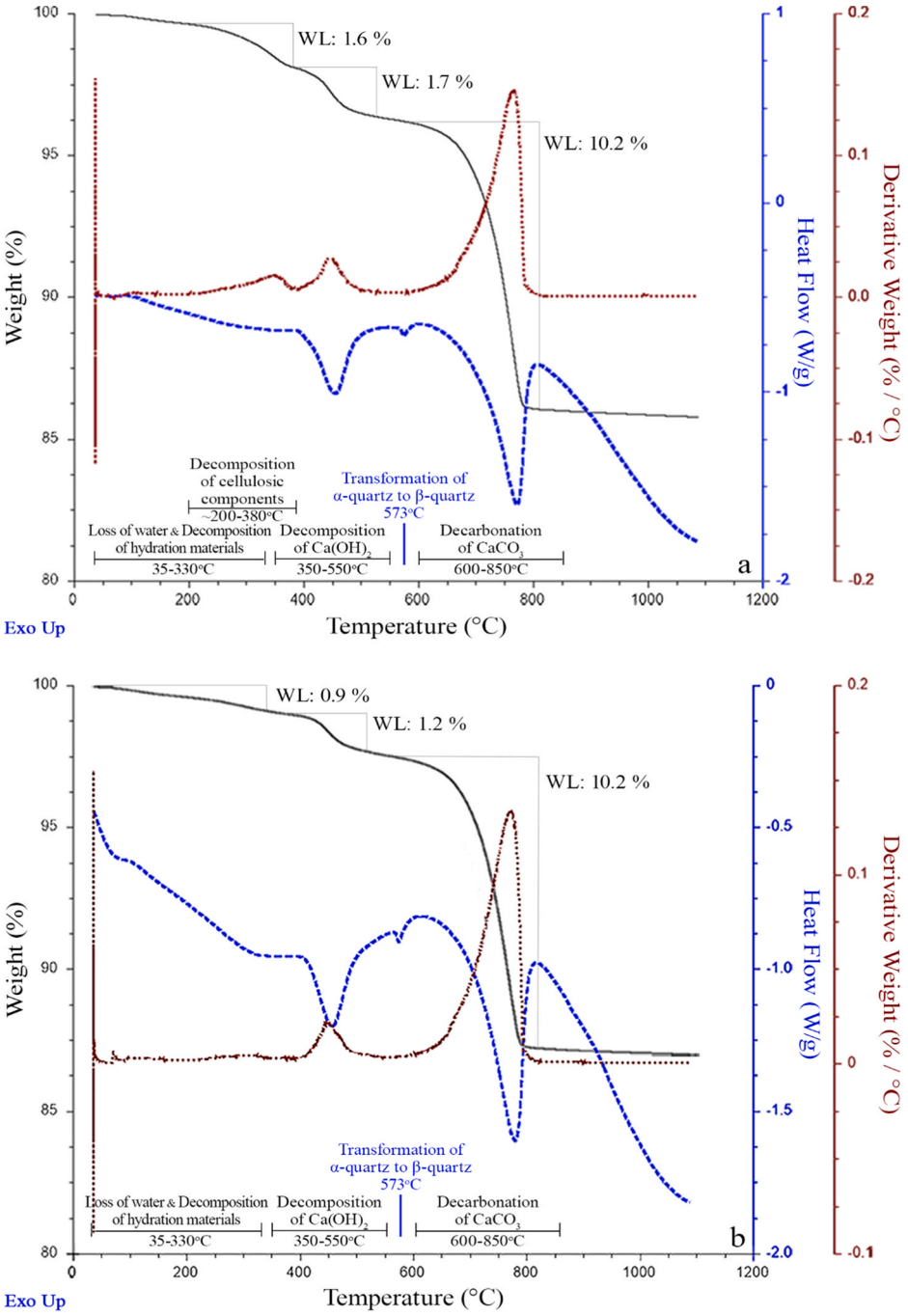

Fig. 12. TGA, DTA, and DTG curves of (a) AH4 and (b) AB4 at 91 days of curing.

(1.65 MPa at 28 days), followed by a reduction at later ages to 1.03 MPa.

These trends align with the microstructural observations: higher fibre dosages increased total porosity and shifted the pore system toward larger capillary pores, weakening both the matrix and fibre–matrix interface. Lower fibre dosages, particularly in CB1 and CH1, helped maintain a finer pore fraction and supported gradual densification, resulting in better retention of long-term strength. Compared with air-lime mortars, the best-performing ternary mixtures were CH1 and CB1. They achieved comparable or higher strengths at 182 days, although they remained well below the NHL series due to the limited hydraulic phase content of the ternary binder.

Fibre and shiv orientation is recognised in the literature as a parameter that can influence mechanical performance of natural-fibre composites [21,27]. Several studies have reported that alignment along the loading direction may enhance compressive strength, whereas different orientations relative to heat flow can alter thermal conductivity. However, in conventionally mixed and cast lime-based composites, precise control of fibre orientation is generally not achievable [21]. In the present study, SEM observations did not indicate any systematic or preferential orientation within the matrix. Consequently, although orientation effects are reported in the literature, no clear evidence of such an influence on compressive strength was identified in this work, likely due to the absence of controlled or dominant fibre alignment.

3.4. Thermogravimetric analyses

Thermogravimetric (TGA) results at 91 days of curing, including differential thermal (DTA) and derivative thermogravimetric (DTG)

Table 5
Weight loss for TG–DTA analysis and specific pore volume (SPV) over 0.1 μm of lime mortars at 91 days.

Samples	Weight Loss (%wt)				SPV (mL/g)
	$Ca(OH)_2$	$CaCO_3$	CO_2/H_2O	Total	> 0.1 μm
N1	1.3	4.2	2.9	8.7	0.43
NH1	0.9	4.1	3.2	7.7	0.41
NH4	0.7	5.0	3.3	8.4	1.06
NB1	1.0	4.1	3.4	7.9	0.45
NB4	0.9	3.7	2.9	7.2	0.31
A1	1.9	8.3	9.8	11.6	1.75
AH1	1.3	13.5	14.5	16.2	1.57
AH4	1.7	10.2	5.6	14.2	1.87
AB1	1.0	12.4	12.7	14.9	1.59
AB4	1.2	10.2	10.3	13.0	1.94
CH1	1.1	11.8	9.5	15.1	1.67
CH4	1.9	9.9	8.9	13.6	1.85
CB1	0.9	16.3	9.5	19.8	1.64
CB4	1.2	10.1	12.1	12.8	1.71

curves, were analysed to assess the hydration and carbonation behaviour of lime-based mortars. The TG-DTA curves revealed distinct weight loss events associated with different thermal decomposition processes (Fig. 12).

The initial mass loss between 35°C and ca. 350°C corresponds to the evaporation of physically bound water and the decomposition of hydration and early pozzolanic reaction products [47,75,76]. Increased losses within this region were recorded in mixtures containing higher amounts of hemp shiv, due to the thermal degradation of cellulosic amorphous constituents, hemicellulose and cellulose, which decompose between 200 and 380°C [77,78]. These effects are clearly reflected in the DTG peaks of mixtures such as AH4 (Fig. 12a). Two major decomposition stages were identified in all mortars. The first, occurring between 350 and 550°C, corresponds to the dehydroxylation of portlandite ($Ca(OH)_2$), while the second, occurring between 600 and 850°C, reflects the decarbonation of $CaCO_3$, both of which produce characteristic endothermic peaks in the DTA curves. In addition, all samples displayed a small endothermic peak at 573°C, attributed to the α-β quartz phase transition originating from the silica sand; this transition does not involve mass loss and therefore does not appear in the TGA curves [79].

The weight losses associated with the decomposition of $Ca(OH)_2$ and $CaCO_3$, along with the total mass losses, and the CO_2/H_2O ratio are summarised in Table 5. The CO_2/H_2O ratio is an indicator of the hydraulic character of the mortars, with hydraulic composites generally showing lower ratios than hydrated ones [80]. It is expected that most hydraulic composites will demonstrate CO_2/H_2O values below 10% which is commonly considered the threshold for moderately hydraulic mortars [81,82]. NHL-based mortars showed CO_2/H_2O values below 10%, confirming their hydraulic character, consistent with the predominance of hydration reactions over carbonation at this curing stage. In all systems, the incorporation of hemp shiv or basalt fibre led to lower mass loss associated with portlandite dehydroxylation, indicating that less unreacted $Ca(OH)_2$ remained after curing, due to predominantly enhanced hydration in NHL mortars, and to increased carbonation in the air-lime and ternary systems. In air lime and ternary mortars, the incorporation of hemp shiv and basalt fibre resulted in lower portlandite contents together with higher $CaCO_3$-related mass losses compared with their respective reference mixture, indicating a more extensive degree of carbonation. Consequently, these mixtures exhibited higher CO_2/H_2O ratios, reflecting a reduced hydraulic character. Notably, only the mixture containing 4 bwob% hemp shiv showed a decrease in the CO_2/H_2O ratio, suggesting a relatively higher hydraulic contribution, which may be associated with the high water-retention capacity of hemp shiv and its influence on internal curing conditions.

This behaviour is consistent with findings in the literature showing that, the pore size distribution of lime composites is a key factor controlling the diffusion of atmospheric CO_2, and that this distribution evolves continuously as carbonation progresses [83,84]. Since CO_2 diffusion is closely tied to pore size and connectivity, changes in pore structure can markedly influence the extent of carbonation over time. Importantly, only pores larger than approximately 0.1 μm actively participate in the carbonation of hydrated lime mortars, whereas finer pores (<0.1 μm) remain largely uninvolved in the reaction [85,86] The specific volumes of pores exceeding 0.1 μm are presented in Table 5. n this study, the hemp- and basalt-reinforced air-lime mortars generally exhibited a higher proportion of these larger pores, originating from poor bonding and interfacial gaps around the reinforcements, as confirmed by microstructural observations. This clarifies the higher carbonation observed in the reinforced mixtures, as a more open pore network allows CO_2 to diffuse more readily into the lime matrix. Additionally, in the hemp-reinforced mixes, the high-water absorption of shives can lower the internal relative humidity, bringing the moisture conditions closer to the optimal range for carbonation to proceed more efficiently [87].

In this context, the differences between hemp- and basalt-reinforced mortars were relatively small, particularly at higher reinforcement dosages, suggesting that the pore-size distribution and the presence of reinforcement, rather than the fibre type itself, played the dominant role in controlling carbonation extent.

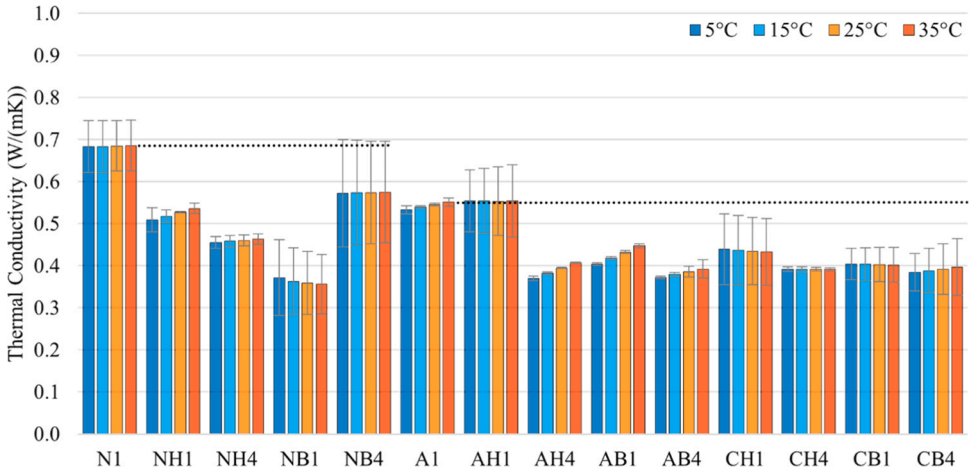

Fig. 13. Thermal conductivity of samples at 91 days of curing, measured at average temperatures of 5, 15, 25, 35 °C. Error bars indicate standard deviation. Dotted lines mark reference sample levels.

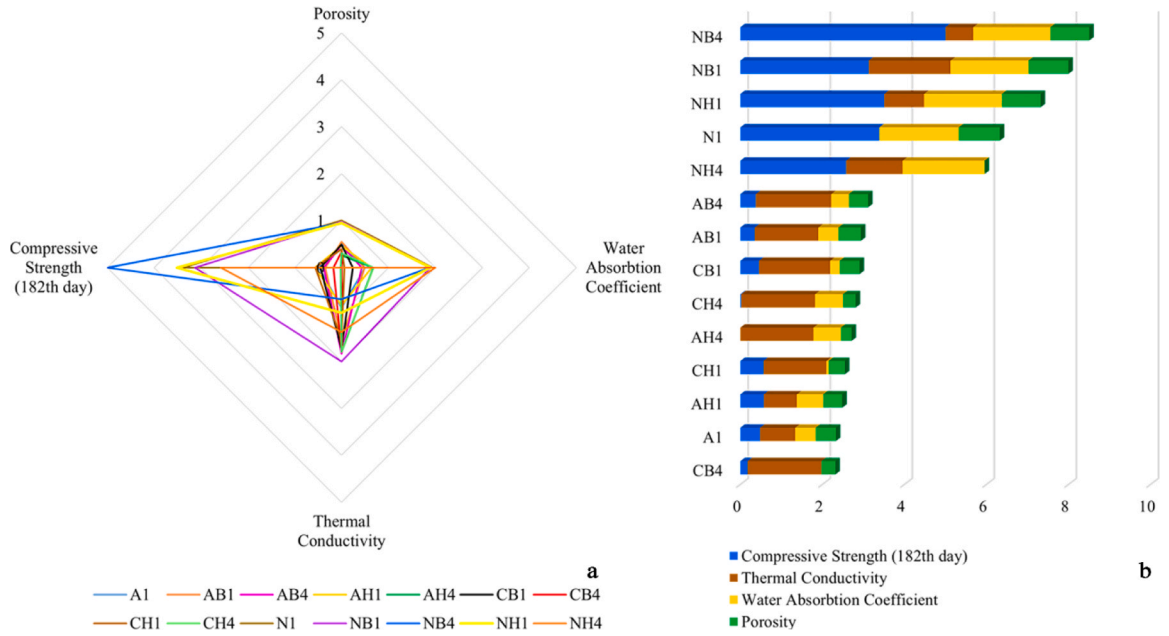

Fig. 14. Weighted property indices for Scenario 1 for each mixture: (a) spider diagram and (b) bar chart showing the contribution of each indicator based on weighted scoring.

3.5. *Thermal conductivity*

Thermal conductivity values measured at 5, 15, 25, and 35°C are shown in Fig. 13. Across all mixtures, thermal conductivity ranged between 0.36 and 0.68 W/(mK). A general increase with temperature was observed, consistent with enhanced heat transfer as thermal energy rises (Fig. 13). This behaviour is attributed to the improved heat carrying capacity of air within the pore network at elevated temperatures [28].

Hemp is a well-established thermal insulator, and numerous studies have reported that its incorporation reduces the thermal conductivity of lime-based composites. Parcesepe et al. [46] documented a 10–15% decrease in NHL mortars reinforced with hemp fibres, while Evangelia et al. [35] observed similar effects in air lime mortars. Hemp shiv has likewise been associated with low thermal conductivity in lime-based binders [28,29,88].

In the present study, hemp shiv addition consistently reduced the thermal conductivity of all lime mortars (Fig. 13), in agreement with existing literature. The effect was most pronounced in natural hydraulic lime mortars, where the addition of 1 bwob% hemp shiv reduced conductivity at 25 °C by 23%, while 4 bwob% yielded a 33% reduction relative to the reference. These reductions were associated with decreases in bulk density of approximately 2% and 15%, respectively. This substantial decrease can be linked to the inherently low porosity and higher thermal conductivity of NHL mortars, conditions under which the introduction of lightweight, porous organic particles markedly increases void volume and reduces heat transfer.

In air lime mortars, AH1 showed conductivity similar to A1, whereas AH4 exhibited a 28% reduction. Ternary mortars showed comparable trends, with CH1 and CH4 presenting reductions of approximately 20% and 28%, respectively. These decreases stem from the insulating nature of hemp and its concomitant increase in pore volume. Particle size also influenced the results: as noted by Mahmood et al. [28], finer shive particles yield lower thermal conductivity, which helps explain the pronounced reduction observed in mixtures containing ground shiv at the 4% dosage.

Basalt fibre is also considered thermally stable and has been associated with improved thermal insulation in cement-based composites [32,89,90]. However, Escamilla et al. [42] reported an increase in conductivity when basalt fibres were added to NHL mortars. In contrast, the present study found that basalt fibre reduced thermal conductivity across all binder systems (Fig. 13). Air lime and ternary mortars containing basalt fibres showed lower conductivity than their respective reference mixes, with more pronounced reductions at the 4 bwob% fibre dosage; 30% in AB4 and 27% in CB4.The greatest improvement occurred in NB1, which exhibited a 47% reduction. Unlike the other systems, increasing basalt fibre content in NHL mortars (NB4) resulted in an increase in conductivity compared to NB1, although NB4 still remained below the reference value (Fig. 13).

3.6. *Weighted scoring framework for holistic performance analysis*

The weighted scoring method was applied to the lime mortars using results for compressive strength (after 182 days of curing), thermal conductivity, water absorption coefficient, and open porosity to evaluate their performance under the selected scenarios. Different weightings (W) were assigned to each performance indicator according to its importance for the intended application of scenarios. For the first scenario (S_1), in which the mortars are used as bedding mortars, the highest weight was assigned to compressive strength (W_{S_1}: 5), followed by thermal conductivity (W_{S_1}: 3) and the water absorption coefficient (W_{S_1}: 3), with porosity (W_{S_1}: 1) assigned the lowest weight. In the second scenario (S_2) to utilise mortars as rendering, the importance was given to thermal conductivity (W_{S_2}: 5), followed by the water absorption coefficient (W_{S_2}: 3), while compressive strength (W_{S_2}: 1) and porosity (W_{S_2}: 1) were assigned lower importance. The overall weighted indices calculated according to the scenario priorities are provided in the Supplementary Material (Table S2 and S3).

In Scenario 1, NB4 exhibited the most favourable performance, owing to its high compressive strength and low water absorption (Fig. 14a) (however, if mechanical resistance is not as important and the aim is to enhance the material's thermal insulation, the NB1 mixture is a very interesting option). This mixture was followed by the other natural hydraulic lime mortars, indicating that natural hydraulic lime–based mortars are particularly suitable for use as bedding mortars. In addition, for each binder type, mixtures reinforced with basalt fibre generally ranked higher than their counterparts containing hemp shiv (Fig. 14b). For structural bedding mortar applications, basalt fibre reinforcement therefore appears to be more suitable than hemp shiv.

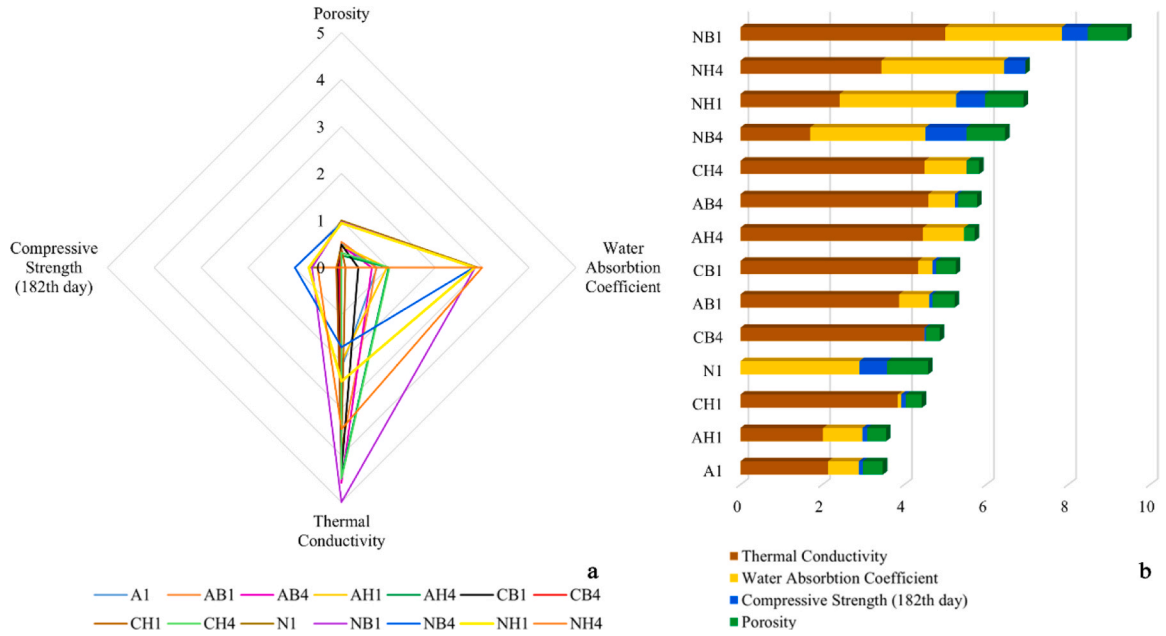

Fig. 15. Weighted property indices for Scenario 2 for each mixture: (a) spider diagram and (b) bar chart showing the contribution of each indicator based on weighted scoring.

On the other hand, utilising these mortars as rendering material has different requirements and different results (Fig. 15). In Scenario 2, NB1 was identified as the best-performing mortar due to its low thermal conductivity (Fig. 15a), which resulted in superior thermal insulation capacity and improved potential energy efficiency in building applications. Even though NHL-based mortars showed higher performance in Scenario 2, as in Scenario 1, air lime and ternary mortars also exhibited improved performance, since compressive strength is of lesser importance for rendering mortars (Fig. 15b). With respect to reinforcement type, it was not clearly evident whether basalt or hemp fibres provide superior performance. Nevertheless, higher reinforcement dosages were found to result in improved performance for rendering mortars (Fig. 15b).

4. Conclusions

This study investigated the influence of hemp shiv and basalt fibre on the physical, microstructural, mechanical and thermal performance of three lime-based mortar systems. Based on the experimental findings, the following conclusions can be drawn:

- Binder type was the primary controlling factor. Natural hydraulic lime (NHL) mortars exhibited the densest microstructure with an average of 1.81 g/mL, lowest capillary absorption, highest compressive strength reaching 10 MPa, and CO_2/H_2O ratios around 3%, confirming their dominant hydraulic character.
- Air lime and ternary mortars showed higher open porosity over 30%, coarser capillary pore networks, and lower strength not exceeding 2 MPa, consistent with carbonation-controlled hardening.
- Hemp shiv increased open porosity and reduced compressive strength, particularly at higher dosages. The macroscopic void formation and weak matrix-shiv interfaces limited long-term mechanical performance in these mortars.
- Hemp shiv reduced the thermal conductivity in all binder systems by up to 33% relative to the reference mixtures, primarily due to its inherent thermal insulation properties and the low shiv–matrix adhesion, which creates additional interfacial pores and increases overall porosity.
- Basalt fibre had limited influence on pore structure but contributed to mechanical enhancement through crack-bridging mechanisms. In NHL mortars, higher fibre dosage produced the highest compressive strength at 182 days (12.8 MPa).
- In air lime and ternary mortars, basalt fibre improved early-age strength but did not sustain long-term gains due to increased porosity and weaker fibre–matrix interfaces.
- Thermal conductivity was inversely correlated with bulk density and positively related to total porosity across all systems.
- Performance suitability depends on application. NHL mortars are more appropriate for the applications requiring higher mechanical resistance, whereas air lime and ternary mortars can be competitive for rendering applications where lower thermal conductivity is prioritised.

Despite the comprehensive experimental programme, this study has some limitations. The investigated mortars were evaluated exclusively at laboratory scale and were not applied under real in situ conditions, which may influence performance due to environmental variability and substrate interactions. Long-term durability under environmental actions such as freeze–thaw cycles, salt crystallisation, and prolonged moisture exposure was not assessed within the scope of this study. In addition, extended ageing beyond 182 days was not performed. Finally, due to laboratory constraints, specimen dimensions deviated from certain standard geometries, which may influence the absolute mechanical values, although consistent methodologies were applied across all mixtures to ensure comparative validity.

Future work should address the long-term durability of these composites under representative environmental actions, including salt crystallisation, and freeze–thaw, as well as the influence of shiv pretreatment on interfacial bonding. Such studies will help refine optimal dosages and mixture designs, supporting the development of lime-based repair mortars that are both compatible with historic substrates and consistent with energy and resource efficiency targets in heritage conservation.

CRediT authorship contribution statement

Loucas Kyriakou: Writing – review & editing, Formal analysis,

PID2020-119975RB-I00 LIMORTHER

Conceptualization. **Elif Çam:** Writing – original draft, Visualization, Validation, Methodology, Investigation, Formal analysis, Data curation, Conceptualization. **José María Fernández:** Writing – review & editing, Conceptualization. **Alvarez José Ignacio:** Writing – review & editing, Supervision, Resources, Project administration, Methodology, Funding acquisition, Conceptualization. **Í ñigo Navarro-Blasco:** Supervision, Resources, Project administration, Methodology, Funding acquisition, Data curation, Conceptualization.

Declaration of Generative AI and AI-assisted technologies in the writing process

During the preparation of this work the authors used ChatGPT (Open AI) for language improvement purposes only. After using this service, the authors reviewed and edited the content as needed and take full responsibility for the content of the published article.

Declaration of Competing Interest

The authors declare that they have no conflict of interest.

Acknowledgements

The present study was carried out with financial support from the Spanish Ministerio de Ciencia e Innovación under the project PID2020–119975RB-I00 (LIMORTHER) and from the European Union through the HORIZON-CL5–2022-D4–02 programme (grant agreement No. 101123293, SINCERE). The authors also acknowledge the contribution of Chaux de Saint-Astier (France) and Calinsa S.A. (Navarra, Spain), who supplied the lime binders used in this work. Elif Çam was supported by a scholarship from the Study Abroad Program of the Ministry of National Education of the Republic of Türkiye, which funded her doctoral training.

Appendix A. Supporting information

Supplementary data associated with this article can be found in the online version at doi:10.1016/j.conbuildmat.2026.146143.

Data availability

Data will be made available on request.

References

[1] N. Davey, A History of Building Materials, Lowe & Brydone Ltd, London, 1961.
[2] J.I. Alvarez, R. Veiga, S. Martínez-Ramírez, M. Secco, P. Faria, P.N. Maravelaki, M. Ramesh, I. Papayianni, J. Válek, RILEM TC 277-LHS report: a review on the mechanisms of setting and hardening of lime-based binding systems, Mater. Struct. /Mater. Et. Constr. 54 (2021), https://doi.org/10.1617/s11527-021-01648-3.
[3] ICOMOS, ICOMOS Charter- Principles for the Analysis, Conservation and Structural Restoration of Architectural Heritage, in: Zimbabwe, 2003.
[4] A.M. Forster, J. Válek, J.J. Hughes, N. Pilcher, Lime binders for the repair of historic buildings: considerations for CO2 abatement, J. Clean. Prod. 252 (2020) 119802, https://doi.org/10.1016/j.jclepro.2019.119802.
[5] K. Elert, C. Rodriguez-Navarro, E.S. Pardo, E. Hansen, O. Cazalla, Lime mortars for the conservation of historic buildings, Stud. Conserv. 47 (2002) 62–75, https://doi.org/10.1179/sic.2002.47.1.62.
[6] D. Zhang, J. Zhao, D. Wang, C. Xu, M. Zhai, X. Ma, Comparative study on the properties of three hydraulic lime mortar systems: Natural hydraulic lime mortar, cement-aerial lime-based mortar and slag-aerial lime-based mortar, Constr. Build. Mater. 186 (2018) 42–52, https://doi.org/10.1016/j.conbuildmat.2018.07.053.
[7] D. Ergenç, R. Fort, M.J. Varas–Muriel, M. Alvarez de Buergo, Mortars and plasters—How to characterize aerial mortars and plasters, Archaeol, Anthropol. Sci. 13 (2021) 1–28, https://doi.org/10.1007/S12520-021-01398-X/FIGURES/6.
[8] C. Groot, R. Veiga, I. Papayianni, R. Van Hees, M. Secco, J.I. Alvarez, P. Faria, M. Stefanidou, RILEM TC 277-LHS report: lime-based mortars for restoration–a review on long-term durability aspects and experience from practice, Mater. Struct. /Mater. Et. Constr. 55 (2022), https://doi.org/10.1617/s11527-022-02052-1.
[9] A. Arizzi, G. Cultrone, Mortars and plasters—how to characterise hydraulic mortars, Archaeol. Anthropol. Sci. 13 (2021) 1–22, https://doi.org/10.1007/S12520-021-01404-2/FIGURES/7.
[10] Asociación Española de Normalización (UNE), UNE-EN 459-1 Building lime Part 1: Definitions, specifications and conformity criteria, 2016. ⟨www.aenor.es⟩.
[11] M. Apostolopoulou, P.G. Asteris, D.J. Armaghani, M.G. Douvika, P.B. Lourenço, L. Cavaleri, A. Bakolas, A. Moropoulou, Mapping and holistic design of natural hydraulic lime mortars, Cem. Concr. Res. 136 (2020) 106167, https://doi.org/10.1016/J.CEMCONRES.2020.106167.
[12] L. De, Á. Rosa, G. Ruiz, R. Moreno, Á. De, L. Rosa, G. Ruiz, R. Moreno, Analysis of the rheological properties of natural hydraulic lime-based suspensions for sustainable construction and heritage conservation, 17, Materials 17 (2024) 825, https://doi.org/10.3390/MA17040825.
[13] P.B. Villanueva, M.I.P. Barrio, A.C. Escamilla, M. de las N.G. García, A.V. Bouzóns, Variations in the physical and mechanical behavior of basalt fiber reinforced NHL mortars exposed to different curing conditions, Case Stud. Constr. Mater. 21 (2024), https://doi.org/10.1016/j.cscm.2024.e03467.
[14] L.C. Lancaster, Mortars and plasters—How mortars were made. The literary sources, Archaeol. Anthropol. Sci. 13 (2021) 1–20, https://doi.org/10.1007/S12520-021-01395-0/TABLES/2.
[15] J.F. González-Sánchez, J.M. Fernández, Navarro-Blasco, J.I. Alvarez, Improving lime-based rendering mortars with admixtures, Constr. Build. Mater. 271 (2021) 121887, https://doi.org/10.1016/j.conbuildmat.2020.121887.
[16] B.A. Silva, A.P. Ferreira Pinto, A. Gomes, Natural hydraulic lime versus cement for blended lime mortars for restoration works, Constr. Build. Mater. 94 (2015) 346–360, https://doi.org/10.1016/j.conbuildmat.2015.06.058.
[17] E.R. Grist, K.A. Paine, A. Heath, J. Norman, H. Pinder, Compressive strength development of binary and ternary lime-pozzolan mortars, Mater. Des. 52 (2013) 514–523, https://doi.org/10.1016/j.matdes.2013.05.006.
[18] F. Kesikidou, M. Stefanidou, Natural fiber-reinforced mortars, J. Build. Eng. 25 (2019) 100786, https://doi.org/10.1016/J.JOBE.2019.100786.
[19] F. Iucolano, B. Liguori, C. Colella, Fibre-reinforced lime-based mortars: a possible resource for ancient masonry restoration, Constr. Build. Mater. 38 (2013) 785–789, https://doi.org/10.1016/j.conbuildmat.2012.09.050.
[20] M. Mercuri, M. Vailati, A. Gregori, Chopped basalt fibers reinforced mortar for strengthening the architectural heritage, 13, Fibers 2025 13 (2025) 20, https://doi.org/10.3390/FIB13020020.
[21] L. Siouta, M. Apostolopoulou, A. Bakolas, Natural fibers in composite materials for sustainable building: a state-of-the-art review on treated hemp fibers and hurds in mortars, Sustainability 16 (2024) 10368, https://doi.org/10.3390/su162310368.
[22] M.L. Santarelli, F. Sbardella, M. Zuena, J. Tirillò, F. Sarasini, Basalt fiber reinforced natural hydraulic lime mortars: A potential bio-based material for restoration, Mater. Des. 63 (2014) 398–406, https://doi.org/10.1016/j.matdes.2014.06.041.
[23] R. Réh, M.C. Barbu, Nonwood bio-based materials / Hemp. Performance of Bio-Based Building Materials, Elsevier Inc, 2017, pp. 105–112, https://doi.org/10.1016/B978-0-08-100982-6.00003-3.
[24] M. Le Troëdec, P. Dalmay, C. Patapy, C. Peyratout, A. Smith, T. Chotard, Mechanical properties of hemp-lime reinforced mortars: Influence of the chemical treatment of fibers, J. Compos. Mater. 45 (2011) 2347–2357, https://doi.org/10.1177/0021998311401088.
[25] S. Avudaiappan, P.I. Cuello Moreno, L.F. Montoya R, M. Chávez-Delgado, K. P. Arunachalam, P. Guindos, T. Marzialetti B, P. Fernando Parra, E.I. Saavedra Flores, J.I. Flores Arrey, Experimental investigation on the physical, microstructural, and mechanical properties of hemp limecrete, Sci. Rep. 13 (2023), https://doi.org/10.1038/s41598-023-48144-y.
[26] N. Mostefai, R. Hamzaoui, S. Guessasma, A. Aw, H. Nouri, Microstructure and mechanical performance of modified hemp fibre and shiv mortars: discovering the

optimal formulation, Mater. Des. 84 (2015) 359–371, https://doi.org/10.1016/j.matdes.2015.06.102.
[27] B. Çomak, A. Bideci, Ö. Salli Bideci, Effects of hemp fibers on characteristics of cement based mortar, Constr. Build. Mater. 169 (2018) 794–799, https://doi.org/10.1016/J.CONBUILDMAT.2018.03.029.
[28] O. Mahmood, M. Kavgic, M. Noel, Hygrothermal and mechanical characterization of novel hemp-lime composites with enhanced consistency, Constr. Build. Mater. 450 (2024), https://doi.org/10.1016/j.conbuildmat.2024.138720.
[29] B. Mazhoud, F. Collet, S. Pretot, J. Chamoin, Hygric and thermal properties of hemp-lime plasters, Build. Environ. 96 (2016) 206–216, https://doi.org/10.1016/j.buildenv.2015.11.013.
[30] A. Bourdot, T. Moussa, A. Gacoin, C. Maalouf, P. Vazquez, C. Thomachot-Schneider, C. Bliard, A. Merabtine, M. Lachi, O. Douzane, H. Karaky, G. Polidori, Characterization of a hemp-based agro-material: influence of starch ratio and hemp shive size on physical, mechanical, and hygrothermal properties, Energy Build. 153 (2017) 501–512, https://doi.org/10.1016/j.enbuild.2017.08.022.
[31] W. Wang, Y. Zhang, Z. Mo, N. Chouw, K. Jayaraman, Z. dong Xu, A critical review on the properties of natural fibre reinforced concrete composites subjected to impact loading, J. Build. Eng. 77 (2023), https://doi.org/10.1016/j.jobe.2023.107497.
[32] C. Ding, K. Xue, G. Yi, Research on fire resistance and economy of basalt fiber insulation mortar, Sci. Rep. 13 (2023), https://doi.org/10.1038/s41598-023-44591-9.
[33] A. Pavlović, T. Donchev, D. Petkova, N. Staletović, Sustainability of alternative reinforcement for concrete structures: Life cycle assessment of basalt FRP bars, Constr. Build. Mater. 334 (2022) 127424, https://doi.org/10.1016/j.conbuildmat.2022.127424.
[34] J. Fořt, J. Kočí, R. Černý, Environmental efficiency aspects of basalt fibers reinforcement in concrete mixtures, Energies 14 (2021) 7736, https://doi.org/10.3390/en14227736.
[35] T. Evangelia, V. Ioanna, M. Stefanidou, Effect of hemp fibers and crystalline admixtures on the properties and self-healing efficiency of lime and clay-based mortars, J. Build. Eng. 86 (2024) 108963, https://doi.org/10.1016/j.jobe.2024.108963.
[36] F. Kesikidou, I. Matamadiotou, M. Stefanidou, Influence of accelerated carbonation on the physico-mechanical properties of natural fiber-reinforced lime mortars, Materials 17 (2024), https://doi.org/10.3390/ma17184461.
[37] A. Bustos, E. Moreno, F. González, A. Cobo, Influence of the addition of carbon fibers on the properties of hydraulic lime mortars: comparison with glass and basalt fibers, Mater. De. Construccion 70 (2020), https://doi.org/10.3989/MC.2020.00120.
[38] D. Asprone, E. Cadoni, F. Iucolano, A. Prota, Analysis of the strain-rate behavior of a basalt fiber reinforced natural hydraulic mortar, Cem. Concr. Compos 53 (2014) 52–58, https://doi.org/10.1016/j.cemconcomp.2014.06.009.
[39] A. Davino, E. Meglio, A. Formisano, Lime-based plaster reinforced with hemp braids as sustainable building product, Architecture 2 (2022) 135–156, https://doi.org/10.3390/architecture2010008.
[40] M. Yıldırım, H.B. Özhan, Durability properties of basalt fiber-reinforced mortars with different mineral admixtures exposed to high temperatures, Constr. Build. Mater. 400 (2023), https://doi.org/10.1016/j.conbuildmat.2023.132574.
[41] Z. Tang, H. Zhang, Y. Pan, L. Ke, Z. Xiang, Z. Lai, Experimental study on mechanical properties of basalt Fiber-Clay lime mortar and application in brick masonry, Constr. Build. Mater. 398 (2023), https://doi.org/10.1016/j.conbuildmat.2023.132479.
[42] A. Cobo Escamilla, P. Bautiste Villanueva, M.I. Prieto Barrio, M. de las N. González García, A. Vázquez Bouzóns, Effect of basalt fiber length on the behavior of natural hydraulic lime-based mortars, Rev. Adv. Mater. Sci. 63 (2024), https://doi.org/10.1515/rams-2023-0191.
[43] A. Bustos-García, E. Moreno-Fernández, F. González-Yunta, A. Cobo-Escamilla, Influencia de la adición de fibras en las propiedades de los morteros de cal hidráulica, Dyna 94 (2018) 228–232, https://doi.org/10.6036/8495.
[44] S. Guler, Z. Funda Akbulut, Workability & mechanical properties of the single and hybrid basalt fiber reinforced volcanic ash-based cement mortars after freeze–thaw cycles, Structures 48 (2023) 1537–1547, https://doi.org/10.1016/j.istruc.2023.01.062.
[45] I. Shah, L. Jing, Z.M. Fei, Y.S. Yuan, M.U. Farooq, N. Kanjana, A review on chemical modification by using sodium hydroxide (NaOH) to investigate the mechanical properties of sisal, coir and hemp fiber reinforced concrete composites, J. Nat. Fibers 19 (2022) 5133–5151, https://doi.org/10.1080/15440478.2021.1875359.
[46] E. Parcesepe, R.F. De Masi, C. Lima, G.M. Mauro, M.R. Pecce, G. Maddaloni, Assessment of mechanical and thermal properties of hemp-lime mortar, Materials 14 (2021) 1–24, https://doi.org/10.3390/ma14040882.
[47] L. Wang, H. Lenormand, H. Zmamou, N. Leblanc, Effect of variability of hemp shiv on the setting of lime hemp concrete, Ind. Crops Prod. 171 (2021) 113915, https://doi.org/10.1016/j.indcrop.2021.113915.
[48] A. Arizzi, G. Cultrone, M. Brümmer, H. Viles, A chemical, morphological and mineralogical study on the interaction between hemp hurds and aerial and natural hydraulic lime particles: implications for mortar manufacturing, Constr. Build. Mater. 75 (2015) 375–384, https://doi.org/10.1016/j.conbuildmat.2014.11.026.
[49] P.B. de Bruijn, K.H. Jeppsson, K. Sandin, C. Nilsson, Mechanical properties of lime-hemp concrete containing shives and fibres, Biosyst. Eng. 103 (2009) 474–479, https://doi.org/10.1016/j.biosystemseng.2009.02.005.
[50] V. Picandet, Particle Size Distribution, in: S. Amziane, F. Collet (Eds.), Bio-Aggregates Based Building Materials, Springer Netherlands, Dordrecht, 2017, pp. 91–110, https://doi.org/10.1007/978-94-024-1031-0.
[51] Asociación Española de Normalización (UNE), UNE-EN 197-1 Cement Part 1: Composition, specifications and conformity criteria for common cements, 2011.
[52] Asociación Española de Normalización (UNE), UNE-EN 196-1 Methods of testing cement Part 1: Determination of strength, 2018.
[53] Lapinus - Rockwool B.V., Product data sheet of Lapinus CF30, (2018). https://doi.org/10.1.
[54] E. Çam, L. Kyriakou, J.M. Fernández, Í. Navarro-Blasco, J.I. Álvarez, Investigating the Influence of Hemp Shiv Size on Air Lime-Based Mortars for Sustainable Restoration Applications, 2025. 4th International Conference on Sustainable Materials, ICSBM, Eindhoven, 2025, pp. 57–59, 2025.
[55] Asociación Española de Normalización (UNE), UNE-EN 1015-3:2000/A2 Methods of test for mortar for masonry. Part 3: Determination of consistence of fresh mortar (by flow table), 2000. ⟨www.aenor.es⟩.
[56] Asociación Española de Normalización (UNE), UNE 83816 Morteros. Métodos de ensayo de los morteros frescos. Determinación de la capacidad de retención de agua, 2021. ⟨www.une.org⟩.
[57] Asociación Española de Normalización (UNE), UNE-EN 1936 Natural stone test methods. Determination of real density and apparent density, and of total and open porosity, 2007.
[58] Asociación Española de Normalización, UNE-EN 15801 Conservation of cultural property. Test methods. Determination of water absorption by capillarity, 2010.
[59] J.M. Kadhim, M. A. Al-Bassam, S.H. Abdas, Materials Selection in Conceptual Design using Weighting Property Method, Eng. Technol. J. 29 (2011) 82–95, https://doi.org/10.30684/etj.29.1.8.
[60] S. Riffi, E. Ghorbel, M. Nouali, T. Imjai, F. Schmidt, F. Cuccagna, Eco-efficient mortars from tunnel excavated soils for wall panels: Performance enhancement and life cycle evaluation, Constr. Build. Mater. 505 (2025) 144682, https://doi.org/10.1016/J.CONBUILDMAT.2025.144682.
[61] N. Kadum, T. Al-Attar, Z. Al-Azzawi, Evaluation of pozzolime mixtures as a sustainable binder to replace portland cement in structural concrete. MATEC Web of Conferences, EDP Sciences, 2017, https://doi.org/10.1051/matecconf/201712002009.
[62] A. Filazi, S. Tortuk, M. Pul, Determination of optimum blast furnace slag ash and hemp fiber ratio in cement mortars, Structures 57 (2023) 105024, https://doi.org/10.1016/J.ISTRUC.2023.105024.
[63] A. Izaguirre, J. Lanas, J.I. Álvarez, Characterization of aerial lime-based mortars modified by the addition of two different water-retaining agents, Cem. Concr. Compos 33 (2011) 309–318, https://doi.org/10.1016/j.cemconcomp.2010.09.008.
[64] B. Silva, A.P. Ferreira Pinto, A. Gomes, A. Candeias, Fresh and hardened state behaviour of aerial lime mortars with superplasticizer, Constr. Build. Mater. 225 (2019) 1127–1139, https://doi.org/10.1016/j.conbuildmat.2019.07.275.
[65] A.R. Santos, M. do, R. Veiga, A. Santos Silva, J. de Brito, J.I. Álvarez, Evolution of the microstructure of lime based mortars and influence on the mechanical behaviour: The role of the aggregates, Constr. Build. Mater. 187 (2018) 907–922, https://doi.org/10.1016/j.conbuildmat.2018.07.223.
[66] J.I. Alvarez, J.M. Fernández, I. Navarro-Blasco, A. Duran, R. Sirera, Microstructural consequences of nanosilica addition on aerial lime binding materials: Influence of different drying conditions, Mater. Charact. 80 (2013) 36–49, https://doi.org/10.1016/J.MATCHAR.2013.03.006.
[67] J. Bartholdy, M.R. Midtgaard, I. Rörig-Dalgaard, M. Taube, Water absorption in medieval lime plaster: Influence of binder ratio, preparation protocol, and limewashing, Constr. Build. Mater. 486 (2025) 141946, https://doi.org/10.1016/J.CONBUILDMAT.2025.141946.
[68] I. Hafhouf, A. Karouche, A. Benalia, C. Roubeche, I. Hitani, M. Duc, A. Sarcinella, M. del Mar Barbero-Barrera, Assessment of ground dune sand (GDS) in the production of air lime mortars for historic buildings restoration, Constr. Build. Mater. 481 (2025) 141604, https://doi.org/10.1016/J.CONBUILDMAT.2025.141604.
[69] S. Divya Rani, A.V. Rahul, M. Santhanam, A multi-analytical approach for pore structure assessment in historic lime mortars, Constr. Build. Mater. 272 (2021) 121905, https://doi.org/10.1016/J.CONBUILDMAT.2020.121905.
[70] P. Pineda, S. Medina-Carrasco, A. Iranzo, L. Borau, I. García-Jiménez, Pore structure and interdisciplinary analyses in Roman mortars: Building techniques and durability factors identification, Constr. Build. Mater. 317 (2022) 125821, https://doi.org/10.1016/J.CONBUILDMAT.2021.125821.
[71] V. Fernandes, L. Silva, V.M. Ferreira, J.A. Labrincha, Evaluation of mixing and application process parameters of single-coat mortars, Cem. Concr. Res. 35 (2005) 836–841, https://doi.org/10.1016/J.CEMCONRES.2004.10.026.
[72] A. Izaguirre, J. Lanas, J.I. Álvarez, Effect of water-repellent admixtures on the behaviour of aerial lime-based mortars, Cem. Concr. Res. 39 (2009) 1095–1104, https://doi.org/10.1016/J.CEMCONRES.2009.07.026.
[73] S. Wang, G. Zhang, Z. Wang, T. Huang, P. Wang, Evolutions in the properties and microstructure of cement mortars containing hydroxyethyl methyl cellulose after controlling the air content, Cem. Concr. Compos 129 (2022) 104487, https://doi.org/10.1016/j.cemconcomp.2022.104487.
[74] J.F. González-Sánchez, B. Taşci, J.M. Fernández, Í. Navarro-Blasco, J.I. Alvarez, Combination of polymeric superplasticizers, water repellents and pozzolanic agents to improve air lime-based grouts for historic masonry repair, Polym. (Basel) 12 (2020), https://doi.org/10.3390/POLYM12040887.
[75] V. Pavlík, M. Užáková, Effect of curing conditions on the properties of lime, lime-metakaolin and lime-zeolite mortars, Constr. Build. Mater. 102 (2016) 14–25, https://doi.org/10.1016/j.conbuildmat.2015.10.128.
[76] R.M.H. Lawrence, T.J. Mays, P. Walker, D. D'Ayala, Determination of carbonation profiles in non-hydraulic lime mortars using thermogravimetric analysis,

Thermochim. Acta 444 (2006) 179–189, https://doi.org/10.1016/j.tca.2006.03.002.
[77] S. Barbhuiya, B. Bhusan Das, A comprehensive review on the use of hemp in concrete, Constr. Build. Mater. 341 (2022) 127857, https://doi.org/10.1016/j.conbuildmat.2022.127857.
[78] M. Chabannes, E. Garcia-Diaz, L. Clerc, J.C. Bénézet, Effect of curing conditions and Ca(OH)2-treated aggregates on mechanical properties of rice husk and hemp concretes using a lime-based binder, Constr. Build. Mater. 102 (2016) 821–833, https://doi.org/10.1016/j.conbuildmat.2015.10.206.
[79] D. Matesová, D. Bonen, Surendra P. Shah, Factors affecting the resistance of cementitious materials at high temperatures and medium[0] heating rates, 39, Mater. Struct. 2006 39 (4) (2006) 455–469, https://doi.org/10.1007/S11527-005-9041-4.
[80] M. Theodoridou, E. Charalambous, P. Maravelaki-Kalaitzaki, I. Ioannou, Amelioration of crushed brick - lime composites using nano-additives, Cem. Concr. Compos 68 (2016) 77–87, https://doi.org/10.1016/J.CEMCONCOMP.2016.02.009.
[81] A. Moropoulou, A. Bakolas, K. Bisbikou, Characterization of ancient, byzantine and later historic mortars by thermal and X-ray diffraction techniques, Thermochim. Acta 269270 (1995) 779–795, https://doi.org/10.1016/0040-6031(95)02571-5.
[82] P. Maravelaki-Kalaitzaki, A. Bakolas, A. Moropoulou, Physico-chemical study of Cretan ancient mortars, Cem. Concr. Res. 33 (2003) 651–661, https://doi.org/10.1016/S0008-8846(02)01030-X.
[83] M. Arandigoyen, J.I. Álvarez, Carbonation process in lime pastes with different water/binder ratio, Mater. De. ConstrucciÓN. 56 (2006) 5–18, https://doi.org/10.3989/MC.2006.V56.I281.88.
[84] E. Ontiveros-Ortega, R. Rodríguez-García, A. González-Serrano, L. Molina, Evolution of mechanical properties in aerial lime mortars of traditional manufacturing, the relationship between putty and powder lime, Constr. Build. Mater. 191 (2018) 575–589, https://doi.org/10.1016/J.CONBUILDMAT.2018.10.053.
[85] R.M. Lawrence, T.J. Mays, S.P. Rigby, P. Walker, D. D'Ayala, Effects of carbonation on the pore structure of non-hydraulic lime mortars, Cem. Concr. Res. 37 (2007) 1059–1069, https://doi.org/10.1016/J.CEMCONRES.2007.04.011.
[86] I. Rigopoulos, L. Kyriakou, M.A. Vasiliades, T. Kyratsi, A.M. Efstathiou, I. Ioannou, Improving the carbonation of air lime mortars at ambient conditions via the incorporation of ball-milled quarry waste, Constr. Build. Mater. 301 (2021) 124073, https://doi.org/10.1016/J.CONBUILDMAT.2021.124073.
[87] R. Haik, G. Bar-Nes, A. Peled, I.A. Meir, Alternative unfired binders as lime replacement in hemp concrete, Constr. Build. Mater. 241 (2020) 117981, https://doi.org/10.1016/j.conbuildmat.2019.117981.
[88] P. Brzyski, M. Gładecki, M. Rumińska, K. Pietrak, M. Kubiś, P. Łapka, Influence of hemp shives size on hygro-thermal and mechanical properties of a hemp-lime composite, 13, Materials 2020 13 (2020) 5383, https://doi.org/10.3390/MA13235383.
[89] M. Asim, G.M. Uddin, H. Jamshaid, A. Raza, Z. ul Rehman, U. Hussain, A.N. Satti, N. Hayat, S.M. Arafat, Comparative experimental investigation of natural fibers reinforced light weight concrete as thermally efficient building materials, J. Build. Eng. 31 (2020) 101411, https://doi.org/10.1016/J.JOBE.2020.101411.
[90] Z.F. Akbulut, S. Guler, Structural self-compacting lightweight concrete: effects of fly ash and basalt fibers on workability, thermal and mechanical properties under ambient conditions and high temperatures, Constr. Build. Mater. 481 (2025) 141658, https://doi.org/10.1016/J.CONBUILDMAT.2025.141658.